Quasiparticle–phonon model of the nucleus. IV. Fragmentation of single-phonon and two-quasiparticle states in spherical nuclei

V. V. Voronov and V. G. Solov'ev

Joint Institute for Nuclear Research, Dubna

Fiz. Elem. Chastits At. Yadra **14**, 1380–1442 (November–December 1983)

The review gives a systematic exposition of the quasiparticle–phonon model of the nucleus as applied to even–even spherical nuclei when the state wave functions are represented as superpositions of single-phonon and two-phonon components. Exact and approximate systems of equations are obtained for determining the energies and coefficients of the wave functions, and expressions are derived for various strength functions. The results are given of calculations of the characteristics of electric giant multipole resonances, neutron and radiative strength functions, and the fragmentation of two-quasiparticle states. Comparison with experiments shows that a good description of the listed characteristics is achieved.

PACS numbers: 21.60.Ev

INTRODUCTION

The problem of describing the fragmentation of the few-quasiparticle components of the wave functions of spherical and deformed nuclei in a wide interval of excitation energies is currently one of the fundamental problems in nuclear theory. The construction of the quasiparticle–phonon model of the nucleus created a basis for systematic investigation of fragmentation. In the framework of the quasiparticle–phonon model one can study the characteristics of complex nuclei due to the fragmentation of single-quasiparticle, single-phonon, and "quasiparticle plus phonon" states. These include neutron and radiative strength functions, photoabsorption cross sections, giant multipole and spin-multipole resonances, and also charge-exchange resonances—and, of course, fragmentation of single-quasiparticle and two-quasiparticle states that are manifested in single-nucleon and two-nucleon transfer reactions. Nonrotational low-lying states in deformed nuclei can be described.

The quasiparticle-phonon model of the nucleus appeared as a result of the development and generalization of the superfluid model of the nucleus.[1–4] Its foundations were laid during 1971–1974 in Refs. 5–10. The general assumptions of the model and some results are given in Refs. 11–17. The results of calculations and comparisons with experimental data have been given in numerous papers (Refs. 18–35).

The development of the quasiparticle–phonon model and its use to calculate the properties of complex nuclei has reached the stage at which it has become necessary to give a detailed mathematical exposition of the model and systematize the results. This is being done in a series of reviews. Some results of investigations of deformed nuclei are given in Refs. 11 and 14, and the situation with regard to single-phonon states in spherical nuclei is described in detail in Ref. 17. The present paper continues this series of reviews. It is devoted to an exposition of the mathematical formalism of the model and the systematization of the results for even–even spherical nuclei.

1. TRANSFORMATION OF THE HAMILTONIAN OF THE MODEL

The Hamiltonian of the quasiparticle–phonon model includes terms that describe the average field of the nucleus in the form of the Woods–Saxon potential, interactions that lead to pairing, and multipole–multipole, spin-multipole–spin-multipole isoscalar and isovector (including charge-exchange) interactions. A general characterization of the Hamiltonian of the model is given in Ref. 10 for deformed nuclei and in Ref. 16 for spherical nuclei. In the present paper, we restrict ourselves to interactions in the particle–hole channel and monopole pairing, ignoring the interactions in the particle–particle channel.

We write the Hamiltonian of the model in the form

$$H = H_{\text{av}} + H_{\text{PAIR}} + H_M^{ph} + H_{SM}^{ph}. \tag{1}$$

Since the average field is given separately for the neutron and proton systems, and the pairing acts only between neutrons and between protons, the terms $H_{\text{av}} + H_{\text{PAIR}}$ are written down separately for the neutron and proton systems. Thus, for the neutron system,

$$H_{\text{av}}^n + H_{\text{PAIR}}^n = \sum_{jm} (E_j - \lambda_n)\, a_{jm}^+ a_{jm} - \frac{G_N}{4} \sum_{jj'} \sum_{mm'} (-)^{j+j'-m-m'} a_{jm}^+ a_{j-m}^+ a_{j'-m'} a_{j'm'}, \tag{2}$$

where E_j are the energies of the single-particle states, characterized by the quantum numbers jm (for brevity, j denotes the set of quantum numbers nlj); a_{jm} and a_{jm}^+ are nucleon creation and annihilation operators; and G_N and G_z are pairing constants. The chemical potentials λ_n and λ_p are determined from the condition of conservation of the number of neutrons and protons on the average.

We write the isoscalar and isovector separable multipole H_M^{ph} and spin-multipole H_{SM}^{ph} interactions in the particle–hole channel in the form

$$H_M^{ph} = -\frac{1}{2} \sum_{\lambda} (\varkappa_0^{(\lambda)} + \varkappa_1^{(\lambda)} \tau_1 \tau_2) \sum_{\mu} M_{\lambda\mu}^+ M_{\lambda\mu}; \tag{3}$$

$$H_{SM}^{ph} = -\frac{1}{2} \sum_{\lambda} \sum_{L=\lambda,\, \lambda\pm1} (\varkappa_0^{(\lambda L)} + \varkappa_1^{(\lambda L)} \tau_1 \tau_2) \sum_{M} (S_{LM}^{\lambda})^+ S_{LM}^{\lambda}, \tag{4}$$

where

$$M_{\lambda\mu}^+ = \sum_{jmj'm'} \langle jm | i^{\lambda} R_{\lambda}(r)\, Y_{\lambda\mu} | j'm' \rangle\, a_{jm}^+ a_{j'm'}; \tag{5}$$

$$(S_{LM}^{\lambda})^+ = \sum_{jmj'm'} \langle jm | i^{\lambda} R_{\lambda}(r)\, [\sigma Y_{\lambda}(\Omega)]_{LM} | j'm' \rangle\, a_{jm}^+ a_{j'm'}; \tag{6}$$

$$[\sigma Y_{\lambda}(\Omega)]_{LM} = \sum_{\mu} \sum_{\rho=0,\,\pm1} \langle 1\rho\lambda\mu | LM \rangle\, \sigma_{\rho} Y_{\lambda\mu}(\Omega).$$

Here, $\varkappa_0^{(\lambda)}$, $\varkappa_1^{(\lambda)}$ and $\varkappa_0^{(\alpha L)}$, $\varkappa_1^{(\alpha L)}$ are the constants of the multipole and spin-multipole isovector and isoscal-

 0090-4759/83/060583-24$04.40

ar forces. To describe the charge-exchange phonons, we use the parts of the interactions (3) and (4) proportional to

$$\varkappa_1^{(\lambda)}(\tau_1^{(+)}\tau_2^{(-)}+\tau_1^{(-)}\tau_2^{(+)}),\quad \varkappa_1^{(\lambda L)}(\tau_1^{(+)}\tau_2^{(-)}+\tau_1^{(-)}\tau_2^{(+)}).$$

The radial dependence $R_\lambda(r)=r^\lambda$ or $R_\lambda(r)\sim\partial V/\partial r$, where V is the central part of the single-particle potential, is discussed in detail in Ref. 16.

To diagonalize the Hamiltonian (2), we make a Bogolyubov canonical transformation:

$$a_{jm}=u_j\alpha_{jm}+(-)^{j-m}v_j\alpha^+_{j-m},$$

i.e., we go over to operators of creation α^+_{jm} and absorption α_{jm} of quasiparticles. The correlation functions C_n and C_p and the chemical potentials λ_n and λ_p (and thus the functions u_j and v_j) can be found from the corresponding equations (see Refs. 4 and 35). From the terms $H_{\text{av}}+H_{\text{PAIR}}$ we retain the terms (see Refs. 4 and 35)

$$\sum_{jm}\varepsilon_j\alpha^+_{jm}\alpha_{jm},\ \varepsilon_j=\sqrt{C^2+(E_j-\lambda)^2} \tag{7}$$

and we ignore the remaining terms, including those responsible for the pairing–vibrational 0^+ states. Since in what follows we shall frequently encounter summation over the quantum numbers of the neutron (n) and proton (p) levels, it is convenient to introduce the notation

$$\sum_\tau A(\tau)=A(n)+A(p),$$

where $\tau=\{n,p\}$ and $\tau\leftrightarrow-\tau$ denotes the substitution $p\leftrightarrow n$. Then

$$\sum_\tau A(\tau)B(\tau)=A(p)B(p)+A(n)B(n);$$
$$\sum_\tau A(\tau)B(-\tau)=A(p)B(n)+A(n)B(p);$$
$$\sum_{\tau,\rho=\pm1}A(\tau)B(\rho\tau)=\sum_\tau[A(\tau)B(\tau)+A(\tau)B(-\tau)].$$

We write the multipole–multipole interaction in the form

$$H_M^{ph}=-\frac{1}{2}\sum_{\lambda\mu}\sum_{\tau\rho=\pm1}(\varkappa_0^{(\lambda)}+\rho\varkappa_1^{(\lambda)})M^+_{\lambda\mu}(\tau)M_{\lambda\mu}(\rho\tau), \tag{8}$$

where

$$\left.\begin{aligned}M^+_{\lambda\mu}(\tau)&=\frac{(-)^{\lambda-\mu}}{\sqrt{2\lambda+1}}\sum_{jj'}{}^{\tau}f^{\lambda}_{jj'}\Big\{\frac{1}{2}u^{(+)}_{jj'}[A^+(jj';\ \lambda\mu)\\&+(-)^{\lambda-\mu}A(jj';\ \lambda-\mu)]+v^{(-)}_{jj'}B_\tau(jj';\ \lambda\mu)\Big\};\\M^+_{\lambda\mu}&=(-)^{\lambda-\mu}M_{\lambda-\mu}.\end{aligned}\right\} \tag{9}$$

In the present paper, we do not consider states of magnetic type and we need only the part of the spin-multipole forces necessary for the formation of the phonon basis. Therefore, we restrict ourselves to the following part of the spin-multipole–spin-multipole interaction:

$$H'^{ph}_{SM}=-\frac{1}{2}\sum_{LM}(\varkappa_0^{(L-1,\ L)}+\varkappa_1^{(L-1,\ L)}\tau_1\tau_2)(S^{L-1}_{LM})^+S^{L-1}_{ML}$$
$$=-\frac{1}{2}\sum_{\substack{LM\\\rho\tau}}(\varkappa_0^{(L-1,\ L)}+\rho\varkappa_1^{(L-1,\ L)})(S^{L-1}_{LM}(\tau))^+S^{L-1}_{LM}(\rho\tau); \tag{10}$$

$$S^{L-1}_{LM}(\tau)=\frac{1}{\sqrt{2L+1}}\sum_{jj'}{}^{\tau}f^{(L-1,\ L)}_{jj'}\ \frac{1}{2}u^{(+)}_{jj'}[A^+(jj';\ L-M)\cdot$$
$$+(-)^{L-M-1}A(jj';\ LM)]+v^{(+)}_{jj'}B_\tau(jj';\ L-M);$$
$$(S^{L-1}_{LM})^+=(-)^{L-M-1}S^{L-1}_{L-M}. \tag{11}$$

In (9) and (11), we have introduced the notation

$$A^+(jj';\ \lambda\mu)=\sum_{mm'}\langle jmj'm'|\lambda\mu\rangle\alpha^+_{jm}\alpha^+_{j'm'};$$

$$B(jj';\ \lambda\mu)=\sum_{mm'}(-)^{j'+m'}\langle jmj'm'|\lambda\mu\rangle\alpha^+_{jm}\alpha_{j'-m'};$$
$$u^{(\pm)}_{jj'}=u_jv_{j'}\pm u_{j'}v_j;\quad v^{(\pm)}_{jj'}=u_ju_{j'}\pm v_jv_{j'};$$
$$f^{(\lambda)}_{jj'}=\langle j\|R_\lambda(r)\,i^\lambda Y_{\lambda\mu}\|j'\rangle\,f^{(\lambda L)}_{jj'}=\langle j\|R_\lambda(r)\,i^\lambda\{\sigma Y_{\lambda\mu}\}_{LM}\|j'\rangle.$$

For the spin-multipole forces in our case $\lambda=L-1$.

To describe the charge-exchange interactions in the particle–hole channel, we use the following parts of the Hamiltonians (3) and (4):

$$H^{ph}_{CM}=-\frac{1}{2}\sum_{\lambda\mu}\varkappa_1^{(\lambda)}M^+_{\lambda\mu}(np)M_{\lambda\mu}(np); \tag{12}$$

$$H^{ph}_{CSM}=-\frac{1}{2}\sum_{LM}\varkappa_1^{(L-1,\ L)}(S^{L-1}_{LM}(np))^+S^{L-1}_{LM}(np); \tag{13}$$

$$M_{\lambda\mu}(np)=\sum_{j_pm_pj_nm_n}\langle j_pm_p\,|\,i^\lambda R_\lambda(r)\,Y_{\lambda\mu}\tau^{(-)}\,|\,j_nm_n\rangle\,a^+_{j_pm_p}a_{j_nm_n}$$
$$=\frac{1}{\sqrt{2\lambda+1}}\sum_{j_pj_n}f^{(\lambda)}_{j_pj_n}\{u_{j_p}v_{j_n}A^+(j_pj_n;\ \lambda-\mu)$$
$$+(-)^{\lambda-\mu}v_{j_p}u_{j_n}A(j_pj_n;\ \lambda\mu) \tag{14}$$
$$+u_{j_p}u_{j_n}B(j_pj_n;\ \lambda-\mu)+(-)^{j_p+j_n-\lambda}v_{j_p}v_{j_n}B(j_nj_p;\ \lambda-\mu)\};$$

$$S^{L-1}_{LM}(np)=\sum_{j_pm_pj_nm_n}\langle j_pm_p\,|\,i^\lambda R_\lambda(r)$$
$$\times[\sigma Y_{\lambda\mu}]_{LM}\tau^{(-)}\,|\,j_nm_n\rangle\,a^+_{j_pm_p}a_{j_nm_n}. \tag{15}$$

Here

$$A^+(j_pj_n;\ \lambda-\mu)=\sum_{m_pm_n}\langle j_pm_pj_nm_n\,|\,\lambda-\mu\rangle\,\alpha^+_{j_pm_p}\alpha^+_{j_nm_n};$$
$$B(j_pj_n;\ \lambda\mu)$$
$$=\sum_{m_pm_n}(-)^{j_n+m_n}\langle j_pm_pj_nm_n\,|\,\lambda\mu\rangle\,\alpha^+_{j_pm_p}\alpha_{j_n-m_n};$$
$$f^{(\lambda)}_{j_pj_n}=\langle j_p\|R_\lambda(r)\,i^\lambda Y_{\lambda\mu}\tau^{(-)}\|j_n\rangle\,f^{(\lambda L)}_{j_pj_n}=\langle j_p\|R_\lambda(r)\,i^\lambda$$
$$\times[\sigma Y_{\lambda\mu}]_{LM}\tau^{(-)}\|j_n\rangle.$$

We introduce phonon operators. We write the creation operator for a phonon of multipolarity λ in the form

$$Q^+_{\lambda\mu i}=\frac{1}{2}\sum_{jj'}\{\psi^{\lambda i}_{jj'}A^+(jj';\lambda\mu)-(-)^{\lambda-\mu}\varphi^{\lambda i}_{jj'}A(jj';\ \lambda-\mu)\}, \tag{16}$$

where the summation over jj' is over the neutron and proton single-particle states. The operators $Q_{\lambda\mu i}$ and $Q^+_{\lambda\mu i}$ satisfy the commutation relations

$$[Q_{\lambda\mu i},\ Q^+_{\lambda'\mu'i'}]$$
$$=\delta_{\lambda\lambda'}\delta_{\mu\mu'}\frac{1}{2}\sum_{jj'}(\psi^{\lambda i}_{jj'}\psi^{\lambda i'}_{jj'}-\varphi^{\lambda i}_{jj'}\varphi^{\lambda i'}_{jj'})$$
$$-\sum_{jj'j_2}\sum_{mm'm_2}\{\psi^{\lambda i}_{j'j_2}\psi^{\lambda'i'}_{jj_2}\langle j'm'j_2m_2\,|\,\lambda\mu\rangle \tag{17}$$
$$\times\langle jmj_2m_2\,|\,\lambda'\mu'\rangle-(-)^{\lambda+\lambda'-\mu-\mu'}\varphi^{\lambda i}_{jj_2}\varphi^{\lambda'i'}_{j'j_2}$$
$$\times\langle jmj_2m_2\,|\,\lambda-\mu\rangle\langle j'm'j_2m_2\,|\,\lambda'-\mu'\rangle\}\,\alpha^+_{jm}\alpha_{j'm'}.$$

The single-phonon state wave function has the form

$$Q^+_{\lambda\mu}\Psi_0; \tag{18}$$

the wave function $\Psi_0\equiv|\,\rangle$ of the ground state of the even–even nucleus is the phonon vacuum:

$$Q_{\lambda\mu i}\Psi_0=0. \tag{19}$$

The conditions of orthonormalization of the wave functions have the form

$$\langle|\,[Q_{\lambda\mu i},\ Q^+_{\lambda'\mu'i'}]\,|\rangle=\delta_{\lambda\lambda'}\delta_{\mu\mu'}\delta_{ii'}. \tag{20}$$

It is generally assumed that the number of quasiparticles in the ground states of even–even nuclei is small, and we therefore set

$$\langle\alpha^+_{jm}\alpha_{jm}\rangle=0. \tag{21}$$

The validity of the condition (21) in various nuclei is in-

vestigated in Ref. 30. In this case, the condition (20) takes the simple form

$$\frac{1}{2}\sum_{jj'}\{\psi^{\lambda i}_{jj'}\psi^{\lambda' i'}_{jj'}-\varphi^{\lambda i}_{jj'}\varphi^{\lambda' i'}_{jj'}\}=\delta_{\lambda\lambda'}\delta_{ii'}; \tag{22}$$

the operators A and A^+ can be expressed in terms of the phonon operators as follows:

$$A(jj';\lambda\mu)=\sum_i\{\psi^{\lambda i}_{jj'}Q_{\lambda\mu i}+(-)^{\lambda-\mu}\varphi^{\lambda i}_{jj'}Q^+_{\lambda-\mu i}\}, \tag{23}$$

where

$$A^+(jj';\lambda\mu)+(-)^{\lambda-\mu}A(jj';\lambda-\mu)$$
$$=\sum_i(\psi^{\lambda i}_{jj'}+\varphi^{\lambda i}_{jj'})(Q^+_{\lambda\mu i}+(-)^{\lambda-\mu}Q_{\lambda-\mu i}). \tag{23'}$$

Thus, all the operators A and A^+ are replaced by phonon operators, and quasiparticles occur in the Hamiltonian only in the form $\alpha^+\alpha$.

We derive equations for determining the energy and structure of multipole single-phonon states. Substituting the expression (23′) in (9) and omitting terms containing the operators B, we obtain after the replacement of (2) by (7)

$$H_I=\sum_{jm}\varepsilon_j\alpha^+_{jm}\alpha_{jm}$$
$$-\frac{1}{8}\sum_{\substack{\lambda\mu\rho\\ \tau ii'}}\frac{1}{2\lambda+1}[\varkappa_0^{(\lambda)}+\rho\varkappa_1^{(\lambda)}]D^{\lambda i}_\tau D^{\lambda i'}_{\rho\tau}$$
$$\times(Q_{\lambda-\mu i}+(-)^{\lambda-\mu}Q^+_{\lambda\mu i})(Q^+_{\lambda-\mu i'}+(-)^{\lambda-\mu}Q_{\lambda\mu i'}), \tag{24}$$

where $D^{\lambda i}_{\rho\tau}=\sum_{jj'}^{\rho\tau}f^{\lambda}_{jj'}u^{(+)}_{jj'}g^{\lambda i}_{jj'}$, in which

$$g^{\lambda i}_{jj'}=\psi^{\lambda i}_{jj'}+\varphi^{\lambda i}_{jj'};\quad \omega^{\lambda i}_{jj'}=\psi^{\lambda i}_{jj'}-\varphi^{\lambda i}_{jj'};\quad \varepsilon_{jj'}=\varepsilon_j+\varepsilon_{j'}.$$

To find the secular equation for the energies $\omega_{\lambda i}$ of the single-phonon states described by the wave function (18), we calculate

$$\langle|\,Q_{\lambda\mu i}H_IQ^+_{\lambda\mu i}\,|\rangle$$
$$=\frac{1}{4}\sum_{jj'}\varepsilon_{jj'}[(g^{\lambda i}_{jj'})^2+(\omega^{\lambda i}_{jj'})^2]$$
$$-\frac{1}{4}\frac{1}{2\lambda+1}\sum_{\rho\tau}(\varkappa_0^{(\lambda)}+\rho\varkappa_1^{(\lambda)})D^{\lambda i}_\tau D^{\lambda i}_{\rho\tau} \tag{25}$$

and use the variational principle in the form

$$\delta\left\{\langle|\,Q_{\lambda\mu i}H_IQ^+_{\lambda\mu i}\,|\rangle-\frac{i\omega_{\lambda i}}{2}\left[\sum_{jj'}g^{\lambda i}_{jj'}\omega^{\lambda i}_{jj'}-2\right]\right\}=0. \tag{26}$$

As a result, we obtain a secular equation and expressions for the phonon amplitudes ψ and φ:

$$(\varkappa_0^{(\lambda)}+\varkappa_1^{(\lambda)})(X^{\lambda i}_M(n)+X^{\lambda i}_M(p))$$
$$-4\varkappa_0^{(\lambda)}\varkappa_1^{(\lambda)}X^{\lambda i}_M(n)X^{\lambda i}_M(p)=1. \tag{27}$$

This is the well-known equation of the random-phase approximation (RPA):

$$X^{\lambda i}_M(\tau)=\frac{1}{2\lambda+1}\sum_{jj'}^{\tau}\frac{(f^{\lambda}_{jj'}u^{(\mp)}_{jj'})^2\varepsilon_{jj'}}{\varepsilon^2_{jj'}-\omega^2_{\lambda i}}; \tag{28}$$

$$\psi^{\lambda i}_{jj'}(\tau)=\frac{1}{\sqrt{2\mathscr{y}^{\lambda i}_\tau}}\frac{f^{(\lambda)}_{jj'}u^{(+)}_{jj'}}{\varepsilon_{jj'}-\omega_{\lambda i}};\quad \varphi^{\lambda i}_{jj'}(\tau)=\frac{1}{\sqrt{2\mathscr{y}^{\lambda i}_\tau}}\frac{f^{(\lambda)}_{jj'}u^{(+)}_{jj'}}{\varepsilon_{jj'}+\omega_{\lambda i}}; \tag{29}$$

$$\left.\begin{aligned}\mathscr{y}^{\lambda i}_\tau&=Y^{\lambda i}_\tau+Y^{\lambda i}_{-\tau}\left\{\frac{1-(\varkappa_0^{(\lambda)}+\varkappa_1^{(\lambda)})X^{\lambda i}_M(\tau)}{(\varkappa_0^{(\lambda)}-\varkappa_1^{(\lambda)})X^{\lambda i}_M(-\tau)}\right\}^2;\\ Y^{\lambda i}_\tau&=\frac{1}{2}\frac{\partial}{\partial\omega}X^{\lambda i}_M(\tau)\Big|_{\omega=\omega_{\lambda i}}\\ &=\frac{1}{2\lambda+1}\sum_{jj'}^{\tau}\frac{(f^{\lambda}_{jj'}u^{(\mp)}_{jj'})^2\varepsilon_{jj'}\omega_{\lambda i}}{(\varepsilon^2_{jj'}-\omega^2_{\lambda i})^2}.\end{aligned}\right\} \tag{30}$$

It is shown in Ref. 4 that for the solutions of (27)

$$\langle|\,Q_{\lambda\mu i'},\ H_IQ^+_{\lambda\mu i}\,|\rangle=\omega_{\lambda i}\delta_{ii'};$$

$$\langle Q_{\lambda-\mu' i},\ Q_{\lambda\mu i}H_I\rangle=\langle H_IQ^+_{\lambda\mu i}Q^+_{\lambda-\mu i}\rangle=0.$$

Therefore, with allowance for the solutions of (27) we can write H_I in the form

$$H_I=\sum_{jm}\varepsilon_j\alpha^+_{jm}\alpha_{jm}+H^{ph}_{Mv};$$
$$H^{ph}_{Mv}=-\frac{1}{4}\sum_{\lambda\mu ii'\tau}\frac{X^{\lambda i}_M(\tau)+X^{\lambda i'}_M(\tau)}{\sqrt{\mathscr{y}^{\lambda i}_\tau\mathscr{y}^{\lambda i'}_\tau}}Q^+_{\lambda\mu i}Q_{\lambda\mu i'}. \tag{31}$$

Using (23′), we separate from the Hamiltonian (8) the part describing the interaction of the quasiparticle with the phonons:

$$H^{ph}_{Mvq}=-\frac{1}{4}\sum_{\lambda\mu i}\sum_{\rho\tau}\left\{\frac{1}{2\lambda+1}[Q_{\lambda-\mu i}+(-)^{\lambda-\mu}Q^+_{\lambda\mu i}](\varkappa_0^{(\lambda)}\right.$$
$$\left.+\rho\varkappa_1^{(\lambda)})D^{\lambda i}_{\rho\tau}\sum_{jj'}^{\tau}f^{\lambda}_{jj'}v^{(\mp)}_{jj'}B_\tau(jj';\lambda-\mu)+\text{h.c.}\right\}.$$

Using the relations that follow from (27)–(29),

$$\frac{1}{2\lambda+1}D^{\lambda i}_\tau=\sqrt{\frac{2}{\mathscr{y}^{\lambda i}_\tau}}X^{\lambda i}_M(\tau);$$
$$\mathscr{y}^{\lambda i}_\tau=\left\{\frac{1-(\varkappa_0^{(\lambda)}+\varkappa_1^{(\lambda)})X^{\lambda i}_M(\tau)}{(\varkappa_0^{(\lambda)}-\varkappa_1^{(\lambda)})X^{\lambda i}_M(-\tau)}\right\}^2\mathscr{y}^{\lambda i}_{-\tau}$$

and the secular equation (27), rewritten in the form

$$\frac{1-(\varkappa_0^{(\lambda)}+\varkappa_1^{(\lambda)})X^{\lambda i}_M(\tau)}{(\varkappa_0^{(\lambda)}-\varkappa_1^{(\lambda)})X^{\lambda i}_M(-\tau)}=\frac{(\varkappa_0^{(\lambda)}-\varkappa_1^{(\lambda)})X^{\lambda i}_M(\tau)}{1-(\varkappa_0^{(\lambda)}+\varkappa_1^{(\lambda)})X^{\lambda i}_M(-\tau)}, \tag{27'}$$

we obtain after some manipulations

$$H^{ph}_{Mvq}=-\frac{1}{2\sqrt{2}}\sum_{\lambda\mu i}\left\{((-)^{\lambda-\mu}Q^+_{\lambda\mu i}+Q_{\lambda-\mu i})\right.$$
$$\left.\times\sum_{jj'\tau}\frac{f^{\lambda}_{jj'}v^{(\mp)}_{jj'}}{\sqrt{\mathscr{y}^{\lambda i}_\tau}}B_\tau(jj';\lambda-\mu)+\text{h.c}\right\}. \tag{32}$$

Since the constants $\varkappa_0^{(\lambda)}$ and $\varkappa_1^{(\lambda)}$ are fixed on solution of the secular equation (27), the interaction of the quasiparticles with the phonons is described without the introduction of new constants. It can be seen from the expression (32) that the interaction is the stronger, the more collectivized is the corresponding phonon, i.e., the smaller the functions $\mathscr{y}^{\lambda i}_n$ and $\mathscr{y}^{\lambda i}_p$.

In the solution of Eq. (27), the diagrams in Fig. 1a are taken into account. Diagrams of the type in Fig. 1b are taken into account in H^{ph}_{Mv} in the solution of Eq. (31). The diagram of Fig. 1c describes the quasiparticle–phonon interaction H^{ph}_{Mvq}.

We obtain a secular equation for the case of spin-multipole phonons and transform the corresponding part of the Hamiltonian of the model. As in the case of multipole phonons, we write

$$H_{II}=\sum_{jm}\varepsilon_j\alpha^+_{jm}\alpha_{jm}-\frac{1}{8}\sum_{LM\rho}\sum_{\tau ii'}\frac{1}{2L+1}[\varkappa_0^{(L-1,L)}$$
$$+\rho\varkappa_1^{(L-1,L)}]D^{Li}_\tau D^{Li'}_{\rho\tau}(Q_{L-Mi}+(-)^{L-M-1}Q^+_{LMi})((-)^{L-M-1}Q_{LMi'}+Q^+_{L-Mi'}) \tag{33}$$

where

$$D^{Li}_\tau=\sum_{jj'}^{\tau}f^{(L-1,L)}_{jj'}u^{(\mp)}_{jj'}\omega^{Li}_{jj'}.$$

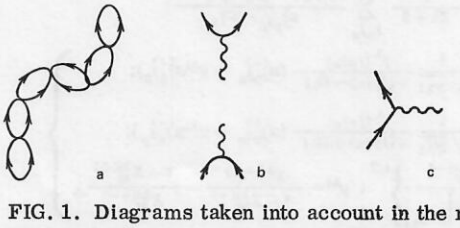

FIG. 1. Diagrams taken into account in the random-phase approximation and in the quasiparticle–phonon interaction.

As in the case of multipole phonons, we obtain a secular equation and coefficients of the wave function for the single-phonon spin-multipole states:

$$(\varkappa_0^{(L-1,\,L)}+\varkappa_1^{(L-1,\,L)})\,[X_S^{Li}(n)+X_S^{L}(p)]$$
$$-4\varkappa_0^{(L-1,\,L)}\varkappa_1^{(L-1,\,L)}X_S^{Li}(n)\,X_S^{Li}(p)=1; \tag{34}$$

$$X_S^{Li}(\tau)=\frac{1}{2L+1}\sum_{jj'}{}^{\tau}\frac{(f_{jj'}^{(L-1,\,L)}u_{jj'}^{(-)})^2\,\varepsilon_{jj'}}{\varepsilon_{jj'}^2-\omega_{Li}^2}; \tag{35}$$

$$\psi_{jj'}^{Li}=\frac{1}{\sqrt{2y_\tau^{Li}}}\frac{f_{jj'}^{(L-1,\,L)}u_{jj'}^{(-)}}{\varepsilon_{jj'}-\omega_{Li}}\quad\varphi_{jj'}^{Li}=\frac{-1}{\sqrt{2y_\tau^{Li}}}\frac{f_{jj'}^{(L-1,\,L)}u_{jj'}^{(-)}}{\varepsilon_{jj'}+\omega_{Li}}; \tag{36}$$

$$\left.\begin{aligned}&y_\tau^{Li}=Y_\tau^{Li}\\&+Y_{-\tau}^{Li}\left\{\frac{1-(\varkappa_0^{(L-1,\,L)}+\varkappa_1^{(L-1,\,L)})\,X_S^{Li}(\tau)}{(\varkappa_0^{(L-1,\,L)}-\varkappa_1^{(L-1,\,L)})\,X_S^{Li}(-\tau)}\right\}^2;\\&Y_\tau^{Li}=\frac{1}{2}\frac{\partial}{\partial\omega}X_S^{Li}(\tau)\Big|_{\omega=\omega_{Li}}\\&=\frac{1}{2L+1}\sum_{jj'}{}^{\tau}\frac{(f_{jj'}^{(L-1,\,L)}u_{jj'}^{(-)})^2\,\varepsilon_{jj'}\omega_{Li}}{(\varepsilon_{jj'}^2-\omega_{Li}^2)^2}.\end{aligned}\right\} \tag{37}$$

Making the same transformations as for the case of the multipole interaction, we obtain

$$H_{Sv}^{ph}=-\frac{1}{4}\sum_{LMii'\tau}\frac{X_S^{Li}(\tau)+X_S^{Li'}(\tau)}{\sqrt{y_\tau^{Li}y_\tau^{Li'}}}Q_{LMi}^{+}Q_{LMi'}; \tag{38}$$

$$H_{Svq}^{ph}=-\frac{1}{2\sqrt{2}}\sum_{LMi}\Big\{(Q_{L-Mi}+(-)^{L-M-1}\,Q_{LMi}^{+})$$
$$\times\sum_{jj'\tau}\frac{f_{jj'}^{(L-1,\,L)}v_{jj'}^{(+)}}{\sqrt{y_\tau^{Li}}}B_\tau(jj';\,L-M)+\text{h.c.}\Big\}. \tag{39}$$

We consider single-phonon charge-exchange multipole states and transform the corresponding part of the Hamiltonian. We write the creation operator for a charge-exchange multipole phonon in the form

$$\Omega_{\lambda\mu i}^{+}=\frac{1}{\sqrt{2}}\sum_{j_pj_n}\Big\{\psi_{j_pj_n}^{\lambda i}A^{+}(j_pj_n;\,\lambda\mu)-(-)^{\lambda-\mu}A(j_pj_n;\,\lambda-\mu)\,\varphi_{j_pj_n}^{\lambda i}\Big\}. \tag{40}$$

We write the sum (7) and the corresponding part of (12) in the form

$$H_{\text{III}}=\sum_{jm}\varepsilon_j\alpha_{jm}^{+}\alpha_{jm}-\frac{1}{16}\sum_{\lambda\mu ii'}\frac{\varkappa_1^{(\lambda)}}{2\lambda+1}\{(D_{+}^{\lambda i}-D_{-}^{\lambda i})\,(-)^{\lambda-\mu}\Omega_{\lambda\mu i}^{+}$$
$$+(D_{+}^{\lambda i}+D_{-}^{\lambda i})\,\Omega_{\lambda-\mu i}\}\{(D_{+}^{\lambda i'}-D_{-}^{\lambda i'})\,(-)^{\lambda-\mu}\Omega_{\lambda\mu i'}$$
$$+(D_{+}^{\lambda i'}+D_{-}^{\lambda i'})\,\Omega_{\lambda-\mu i'}^{+}\},$$

where

$$D_{+}^{\lambda i}=\sum_{j_pj_n}f_{j_pj_n}^{(\lambda)}u_{j_pj_n}^{(+)}g_{j_pj_n}^{\lambda i}\quad D_{-}^{\lambda i}=\sum_{j_pj_n}f_{j_pj_n}^{(\lambda)}u_{j_pj_n}^{(-)}\omega_{j_pj_n}^{\lambda i}.$$

We find the expectation value of H_{III} with respect to the single-phonon state

$$\Omega_{\lambda\mu i}^{+}\Psi_0 \tag{41}$$

and by means of the variational principle obtain a secular equation for finding the energies $\Omega_{\lambda i}$:

$$\mathcal{F}_{CM}(\Omega)\equiv(1-\varkappa_1^{(\lambda)}X_M^{(+)})\,(1-\varkappa_1^{(\lambda)}X_M^{(-)})-(\varkappa_1^{(\lambda)})^2\,(X_M^{(+-)})^2=0, \tag{42}$$

where

$$X_M^{(\pm)}=\frac{2}{2\lambda+1}\sum_{j_pj_n}\frac{(f_{j_pj_n}^{(\lambda)}u_{j_pj_n}^{(\pm)})^2\,\varepsilon_{j_pj_n}}{\varepsilon_{j_pj_n}^2-\Omega_{\lambda i}^2};$$

$$X_M^{(+-)}=\frac{2}{2\lambda+1}\sum_{j_pj_n}\frac{(f_{j_pj_n}^{(\lambda)})^2\,u_{j_pj_n}^{(+)}u_{j_pj_n}^{(-)}\Omega_{\lambda i}}{\varepsilon_{j_pj_n}^2-\Omega_{\lambda i}^2};$$

$$\left.\begin{aligned}&\psi_{j_pj_n}^{\lambda i}=\sqrt{\frac{\varkappa_1^{(\lambda)}}{2\lambda+1}}\frac{1}{\sqrt{y_{\lambda i}}}\frac{f^{\lambda}(j_pj_n)}{\varepsilon(j_pj_n)-\Omega_{\lambda i}}(u_{j_pj_n}^{(+)}+y^{\lambda i}u_{j_nj_p}^{(-)});\\&\varphi_{j_pj_n}^{\lambda i}=\sqrt{\frac{\varkappa_1^{(\lambda)}}{2\lambda+1}}\frac{1}{\sqrt{y_{\lambda i}}}\frac{f^{\lambda}(j_pj_n)}{\varepsilon(j_pj_n)+\Omega_{\lambda i}}(u_{j_pj_n}^{(+)}-y^{\lambda i}u_{j_nj_p}^{(-)});\\&\frac{1}{\sqrt{y_{\lambda i}}}=\left\{\frac{1-X_M^{\lambda i(-)}}{-\dfrac{\partial\mathcal{F}_{CM}}{\partial\Omega}\Big|_{\Omega=\Omega_{\lambda i}}}\right\}^{1/2};\quad y^{\lambda i}=\frac{X^{\lambda i(+-)}}{1-X_M^{\lambda i(-)}}=\frac{1-X_M^{\lambda i(+)}}{X_M^{\lambda i(+-)}},\end{aligned}\right\} \tag{43}$$

in which $\mathcal{y}_{\lambda i}$ is the value of the derivative with respect to Ω of the left-hand side of (42) at $\Omega=\Omega_{\lambda i}$.

In this case, taking into account the solutions of (42) we have

$$\langle|\,\Omega_{\lambda\mu i}H_{\text{III}}\Omega_{\lambda\mu i}^{+}\,|\rangle=\Omega_{\lambda i},$$

the coefficients in H_{III} vanishing for $\Omega_{\lambda\mu i}^{+}\Omega_{\lambda-\mu i}^{+}$, $\Omega_{\lambda-\mu i}\Omega_{\lambda\mu i}$, and also in the case $i\neq i'$ for $\Omega_{\lambda\mu i}^{+}\Omega_{\lambda\mu i}$. Further,

$$H_{CMv}=-\sum_{\lambda\mu ii'}\frac{1+y^{\lambda i}y^{\lambda i'}}{\sqrt{\mathcal{y}_{\lambda i}\mathcal{y}_{\lambda i'}}}\Omega_{\lambda\mu i}^{+}\Omega_{\lambda\mu i'}; \tag{44}$$

$$H_{CMvq}=-\sum_{\lambda\mu i}\sqrt{\frac{\varkappa_1^{(\lambda)}}{\mathcal{y}_{\lambda i}}}\sum_{j_pj_n}\frac{f^{\lambda}(j_pj_n)}{\sqrt{2\lambda+1}}\{[(-)^{\lambda-\mu}(1-y^{\lambda i})\,\Omega_{\lambda\mu i}^{+}$$
$$+(1+y^{\lambda i})\,\Omega_{\lambda-\mu i}]\,[u_{j_p}u_{j_n}B(j_pj_n;\,\lambda-\mu)$$
$$+(-)^{j_p+j_n-\lambda}v_{j_p}v_{j_n}B(j_nj_p;\,\lambda-\mu)]+\text{h.c.}\}. \tag{45}$$

The expressions for H_{CSv} and H_{CSvq} for the charge-exchange spin-multipole interactions differ from (44) and (45) in that the reduced matrix elements of the multipole operators in them are replaced by the matrix elements of the spin-multipole operators.

Thus, the Hamiltonian of the model with allowance for the secular equations (27), (34), and (42), which determine the energies of the single-phonon states, has the form

$$H_M=\sum_{jm}\varepsilon_j\alpha_{jm}^{+}\alpha_{jm}+H_{Mv}^{ph}+H_{Mvq}^{ph}+H_{Sv}^{ph}$$
$$+H_{Svq}^{ph}+H_{CMv}^{ph}+H_{CMvq}^{ph}+H_{CSv}^{ph}+H_{CSvq}^{ph}. \tag{46}$$

2. SYSTEMS OF BASIC EQUATIONS AND THEIR SOLUTIONS

In the quasiparticle–phonon model one can describe the properties of even–even spherical nuclei due to fragmentation of single-phonon or two-quasiparticle states. The wave function of excited states can be written in the form

$$\Psi_\nu(JM)=\Big[\sum_i R_i(J\nu)\,Q_{JMi}^{+}$$
$$+\sum_{\substack{\lambda_1i_1\\\lambda_2i_2}}P_{\lambda_2i_2}^{\lambda_1i_1}(J\nu)\,[Q_{\lambda_1\mu_1i_1}^{+}Q_{\lambda_2\mu_2i_2}^{+}]_{JM}\Big]\Psi_0, \tag{47}$$

where

$$[Q_{\lambda_1\mu_1i_1}^{+}Q_{\lambda_2\mu_2i_2}^{+}]_{JM}=\sum_{\mu_1\mu_2}\langle\lambda_1\mu_1\lambda_2\mu_2\,|\,JM\rangle\,Q_{\lambda_1\mu_1i_1}^{+}Q_{\lambda_2\mu_2i_2}^{+}.$$

Here, JMi and $\lambda\mu i$ denote the quantum numbers of the multipole and spin-multipole phonons. We have restricted ourselves in (47) to the two-phonon terms, and later it will be necessary to add the three-phonon terms. The normalization condition can be written as

$$\sum_i(R_i(J\nu))^2+2\sum_{\substack{\lambda_1i_1\\\lambda_2i_2}}(P_{\lambda_2i_2}^{\lambda_1i_1}(J\nu))^2$$
$$+\sum_{\lambda_1i_1\lambda_2i_2}\sum_{\lambda_1'i_1'\lambda_2'i_2'}P_{\lambda_2'i_2'}^{\lambda_1'i_1'}(J\nu)\,P_{\lambda_2i_2}^{\lambda_1i_1}(J\nu)$$
$$\times K^{J}(\lambda_2'i_2',\,\lambda_1'i_1'\,|\,\lambda_1i_1,\,\lambda_2i_2)=1. \tag{48}$$

Here

$$\sum_{\substack{\mu\mu_2\\\mu'\mu_2'}}\langle\lambda'\mu'\lambda_2'\mu_2'\,|\,JM\rangle\,\langle\lambda\mu\lambda_2\mu_2\,|\,J\mu\rangle$$
$$\times\langle Q_{\lambda_2'\mu_2'i_2'}Q_{\lambda'\mu'i'}Q_{\lambda\mu i}^{+}Q_{\lambda_2\mu_2i_2}^{+}\rangle=\delta_{\lambda\lambda'}\delta_{ii'}\delta_{\lambda_2\lambda_2'}\delta_{i_2i_2'}$$
$$+\delta_{\lambda\lambda_2'}\delta_{ii_2'}\delta_{\lambda_2\lambda'}\delta_{i_2i'}+K^{J}(\lambda_2'i_2',\,\lambda'i'\,|\,\lambda i,\,\lambda_2i_2), \tag{49}$$

where

$$K^J(\lambda_2' i_2', \lambda' i' \mid \lambda i, \lambda_2 i_2)$$

$$= \sum_{\substack{\mu\mu_2 \\ \mu'\mu_2'}} \langle \lambda'\mu'\lambda_2'\mu_2' \mid JM\rangle \langle \lambda\mu\lambda_2\mu_2 \mid JM\rangle K(\lambda_2'\mu_2' i_2', \lambda'\mu' i' \mid \lambda\mu i, \lambda_2\mu_2 i_2); \quad (50)$$

$$K(\lambda_2'\mu_2' i_2', \lambda'\mu' i' \mid \lambda\mu i, \lambda_2\mu_2 i_2)$$

$$= \sum_{\substack{j_1 j_2 j_3 j_4 \\ m_1 m_2 m_3 m_4}} \{\psi^{\lambda' i'}_{j_3 j_4} \psi^{\lambda i}_{j_1 j_4} \langle j_3 m_3 j_4 m_4 \mid \lambda'\mu'\rangle \langle j_1 m_1 j_4 m_4 \mid \lambda\mu\rangle$$

$$- (-)^{\lambda+\lambda'-\mu-\mu'} \varphi^{\lambda' i'}_{j_1 i_4} \varphi^{\lambda i}_{j_3 j_4} \langle j_1 m_1 j_4 m_4 \mid \lambda' -\mu'\rangle \langle j_3 m_3 j_4 m_4 \mid \lambda -\mu\rangle\}$$

$$\times \{\psi^{\lambda_2 i_2}_{j_2 j_3} \psi^{\lambda_2' i_2'}_{j_1 j_2} \langle j_3 m_3 j_2 m_2 \mid \lambda_2\mu_2\rangle \langle j_1 m_1 j_2 m_2 \mid \lambda_2'\mu_2'\rangle$$

$$+ (-)^{\lambda_2+\lambda_2'-\mu_2-\mu_2'} \varphi^{\lambda_2 i_2}_{j_1 j_2} \varphi^{\lambda_2' i_2'}_{j_3 j_2} \langle j_1 m_1 j_2 m_2 \mid \lambda_2 -\mu_2\rangle \langle j_3 m_3 j_2 m_2 \mid \lambda_2' -\mu_2'\rangle\}. \quad (51)$$

We shall find the most general form of the equations of the model. For simplicity, we restrict ourselves to multipole–multipole interactions, i.e., in the Hamiltonian of the model (46) we take the first three terms. Then we add others. We calculate the expectation value of H_I with respect to (47) and obtain as a result

$$(\Psi_\nu^*(JM)\, H_I \Psi_\nu(JM))$$

$$= \sum_i \omega_{Ji} R_i^2(J\nu) + \sum_{\substack{\lambda_1 i_1 \lambda_2 i_2 \\ \lambda_1' i_1' \lambda_2' i_2'}} P^{\lambda_1' i_1'}_{\lambda_2' i_2'}(J\nu)\, P^{\lambda_1 i_1}_{\lambda_2 i_2}(J\nu) \Big\{ (\omega_{\lambda_1 i_1} + \omega_{\lambda_2 i_2})$$

$$\times [\delta_{\lambda_1\lambda_1'}\delta_{i_1 i_1'}\delta_{\lambda_2\lambda_2'}\delta_{i_2 i_2'} + \delta_{\lambda_1\lambda_2'}\delta_{i_1 i_2'}\delta_{\lambda_2\lambda_1'}\delta_{i_2 i_1'} + K^J(\lambda_2' i_2', \lambda_1' i_1' \mid \lambda_1 i_1, \lambda_2 i_2)]$$

$$- \frac{1}{4} \sum_{i_3\tau} \left[\frac{X_M^{\lambda_1' i_1'}(\tau) + X_M^{\lambda_1' i_3}(\tau)}{\sqrt{y_\tau^{\lambda_1' i_1'} y_\tau^{\lambda_1' i_3}}} K^J(\lambda_2' i_2', \lambda_1' i_3 \mid \lambda_1 i_1, \lambda_2 i_2) \right.$$

$$\left. + \frac{X_M^{\lambda_2' i_2'}(\tau) + X_M^{\lambda_2' i_3}(\tau)}{\sqrt{y_\tau^{\lambda_2' i_2'} y_\tau^{\lambda_2' i_3}}} K^J(\lambda_2' i_3, \lambda_1' i_1' \mid \lambda_1 i_1, \lambda_2 i_2) \right]$$

$$- \frac{1}{4} \sum_{\substack{\lambda_3 i_3 i_3' \\ \lambda_4 i_4 \tau}} \frac{X_M^{\lambda_3 i_3}(\tau) + X_M^{\lambda_3 i_3'}(\tau)}{\sqrt{y_\tau^{\lambda_3 i_3} y_\tau^{\lambda_3 i_3'}}}$$

$$\times K^J(\lambda_4 i_4, \lambda_3 i_3' \mid \lambda_1 i_1, \lambda_2 i_2)\, K^J(\lambda_2' i_2', \lambda_1' i_1' \mid \lambda_3 i_3, \lambda_4 i_4) \Big\}$$

$$+ 2 \sum_{\lambda_1 i_1 \lambda_2 i_2 i} R_i(J\nu)\, P^{\lambda_1 i_1}_{\lambda_2 i_2}(J\nu) \{U^{\lambda_1 i_1}_{\lambda_2 i_2}(Ji) + V^{\lambda_1 i_1}_{\lambda_2 i_2}(Ji)\}, \quad (52)$$

where

$$U^{\lambda_1 i_1}_{\lambda_2 i_2}(Ji) = \langle \mid Q_{JMi} (H^{ph}_{Mvq} + H^{ph}_{Svq}) [Q^+_{\lambda_1\mu_1 i_1} Q^+_{\lambda_2\mu_2 i_2}]_{JM} \mid \rangle$$

$$\equiv \sum_\tau U^{\lambda_1 i_1}_{\lambda_2 i_2}(Ji, \tau); \quad (53)$$

$$U^{\lambda_1 i_1}_{\lambda_2 i_2}(Ji, \tau) = (-)^{\lambda_1+\lambda_2-J} \frac{1}{\sqrt{2}} [(2\lambda_1+1)(2\lambda_2+1)]^{1/2}$$

$$+ \sum_{j_1 j_2 j_3}^{\tau} \left[\frac{f^J_{j_1 j_3} v^{(\mp)}_{j_1 j_2}}{\sqrt{y^{Ji}_\tau}} \left\{ \begin{matrix} \lambda_1 \lambda_2 J \\ j_1 j_2 j_3 \end{matrix} \right\} (\psi^{\lambda_1 i_1}_{j_3 j_1} \varphi^{\lambda_2 i_2}_{j_3 j_2} + (-)^{b_J} \psi^{\lambda_2 i_2}_{j_3 j_2} \varphi^{\lambda_1 i_1}_{j_3 j_1}) \right.$$

$$+ \frac{f^{\lambda_1 i_1}_{j_1 j_2} v^{(\mp)}_{j_1 j_2}}{\sqrt{y^{\lambda_1 i_1}_\tau}} \left\{ \begin{matrix} \lambda_1 \lambda_2 J \\ j_3 j_2 j_1 \end{matrix} \right\} (\varphi^{Ji}_{j_3 j_2} \varphi^{\lambda_2 i_2}_{j_3 j_1} + (-)^{b_1} \psi^{Ji}_{j_3 j_2} \psi^{\lambda_2 i_2}_{j_3 j_1})$$

$$\left. + \frac{f^{\lambda_2 i_2}_{j_1 j_2} v^{(\mp)}_{j_1 j_2}}{\sqrt{y^{\lambda_2 i_2}_\tau}} \left\{ \begin{matrix} \lambda_1 \lambda_2 J \\ j_1 j_3 j_2 \end{matrix} \right\} (\psi^{Ji}_{j_3 j_1} \psi^{\lambda_2 i_2}_{j_3 j_3} + (-)^{b_2} \varphi^{Ji}_{j_3 j_1} \varphi^{\lambda_2 i_2}_{j_3 j_3}) \right], \quad (53')$$

where $v^{(1)}_{j_1 j_2}$ appears in conjunction with the multipole matrix elements $f^J_{j_1 j_2}$, $f^\lambda_{j_1 j_2}$, and $v^{(+)}_{j_1 j_2}$ with the spin-multipole elements; the numbers b_J and b_k take the value 0 in the case of the multipole matrix elements $f^J_{j_1 j_2}$, $f^{\lambda k}_{j_1 j_2}$ and 1 in the case of the spin-multipole elements. To the function U there corresponds the diagram in Fig. 2a. The function V vanishes for $K^J = 0$, and to it there correspond diagrams b and c in Fig. 2.

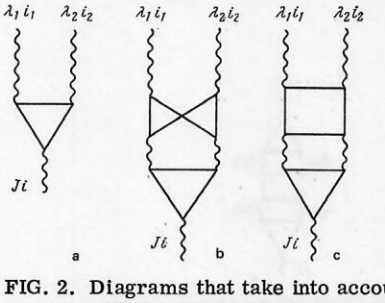

FIG. 2. Diagrams that take into account the coupling of the single-phonon and two-phonon states.

We use the variational principle in the form

$$\delta\{(\Psi_\nu^*(JM)\, H_M \Psi_\nu(JM)) - \eta_\nu [(\Psi_\nu^*(JM)\, \Psi_\nu(JM)) - 1]\} = 0 \quad (54)$$

and obtain a system of two equations. From the first equation

$$(\omega_{Ji} - \eta_\nu) R_i(J\nu) + \sum_{\lambda_1 i_1 \lambda_2 i_2} P^{\lambda_1 i_1}_{\lambda_2 i_2}(J\nu) \{U^{\lambda_1 i_1}_{\lambda_2 i_2}(Ji) + V^{\lambda_1 i_1}_{\lambda_2 i_2}(Ji)\} = 0$$

we find $R_i(J\nu)$, substitute in the second, and obtain a secular equation for determining the energies η_ν in the form of a determinant in the space of two-phonon states:

$$\det \Big\| (\omega_{\lambda_1 i_1} + \omega_{\lambda_2 i_2} - \eta) [\delta_{\lambda_1\lambda_1'}\delta_{i_1 i_1'}\delta_{\lambda_2\lambda_2'}\delta_{i_2 i_2'}$$

$$+ \delta_{\lambda_1\lambda_2'}\delta_{i_1 i_2'}\delta_{\lambda_2\lambda_1'}\delta_{i_2 i_1'} + K^J(\lambda_2' i_2', \lambda_1' i_1' \mid \lambda_1 i_1, \lambda_2 i_2)]$$

$$- \frac{1}{4} \sum_{i_3\tau} \left[\frac{X_M^{\lambda_1' i_1'}(\tau) + X_M^{\lambda_1' i_3}(\tau)}{\sqrt{y_\tau^{\lambda_1' i_1'} y_\tau^{\lambda_1' i_3}}} K^J(\lambda_2' i_2', \lambda_1' i_3 \mid \lambda_1 i_1, \lambda_2 i_2) \right.$$

$$\left. + \frac{X_M^{\lambda_2' i_2'}(\tau) + X_M^{\lambda_2' i_3}(\tau)}{\sqrt{y_\tau^{\lambda_2' i_2'} y_\tau^{\lambda_2' i_3}}} K^J(\lambda_2' i_3, \lambda_1' i_1' \mid \lambda_1 i_1, \lambda_2 i_2) \right]$$

$$- \frac{1}{4} \sum_{\substack{\lambda_3 i_3 i_3' \\ \lambda_4 i_4 \tau}} \frac{X_M^{\lambda_3 i_3}(\tau) + X_M^{\lambda_3 i_3'}(\tau)}{\sqrt{y_\tau^{\lambda_3 i_3} y_\tau^{\lambda_3 i_3'}}}$$

$$\times K^J(\lambda_4 i_4, \lambda_3 i_3' \mid \lambda_1 i_1, \lambda_2 i_2)\, K^J(\lambda_2' i_2', \lambda_1' i_1' \mid \lambda_3 i_3, \lambda_4 i_4)$$

$$- \sum_i \frac{(U^{\lambda_1 i_1}_{\lambda_2 i_2}(Ji) + V^{\lambda_1 i_1}_{\lambda_2 i_2}(Ji))\, (U^{\lambda_1' i_1'}_{\lambda_2 i_2}(Ji) + V^{\lambda_1' i_1'}_{\lambda_2 i_2}(Ji))}{\omega_{Ji} - \eta_\nu} \Big\| = 0. \quad (55)$$

The rank of this determinant is equal to the number of two-phonon terms in the wave function (47).

We illustrate Eq. (55) in the language of diagrams. In the first term, we take into account the diagrams in Figs. 3a and 3b, and we then take into account diagrams c and d. Diagram e corresponds to the terms containing $U \cdot U$, diagram f to the terms containing $U \cdot V$, and diagram g to the terms containing $V \cdot V$. In addition, there are diagrams obtained from diagrams c, d, f, and g by replacing the part a by b. The nominal nature of this illustration must be borne in mind, especially since

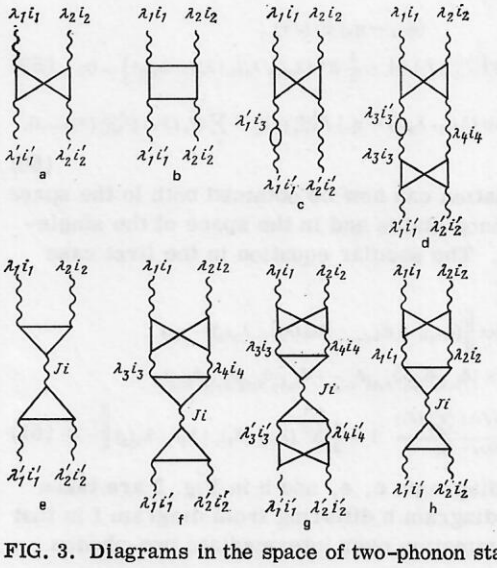

FIG. 3. Diagrams in the space of two-phonon states.

the vertex parts are different in each case.

The secular equation (55) is very complicated—for medium and heavy nuclei, the rank of this determinant is 10^3–10^5. It can be solved if the single-phonon basis is drastically truncated. We have here taken into account many graphs that make a very small contribution to the fragmentation of the single-phonon states. And to calculate the fragmentation of the two-phonon states, it is necessary to take into account the three-phonon terms of the wave function. We therefore go over to an approximate system of equations. For this, we first restrict ourselves in the expression (52) to the terms proportional to $[P^{\lambda_1 i_1}_{\lambda_2 i_2}(J\nu)]^2$ and, second, in the term quadratic in K^J we take one of the K^J in diagonal form. This restriction can be made in (52) because the absolute values of the diagonal terms of K^J are appreciably greater than those of the nondiagonal terms. We also restrict ourselves to the diagonal values of K^J in the normalization condition (48). As a result, we obtain

$$\sum_i (R_i(J\nu))^2 + 2\sum_{\lambda_1 i_1 \lambda_2 i_2} (P^{\lambda_1 i_1}_{\lambda_2 i_2}(J\nu))^2 \left\{1+\frac{1}{2}K^J(\lambda_2 i_2, \lambda_1 i_1 \mid \lambda_1 i_1, \lambda_2 i_2)\right\} = 1; \quad (56)$$

$$(\Psi^*_\nu(JM) H_M \Psi_\nu(JM)) = \sum_i \omega_{Ji} R_i^2(J\nu) + 2\sum_{\lambda_1 i_1 \lambda_2 i_2} (P^{\lambda_1 i_1}_{\lambda_2 i_2}(J\nu))^2 (1+K^J(\lambda_2 i_2, \lambda_1 i_1 \mid \lambda_1 i_1, \lambda_2 i_2)) \times (\omega_{\lambda_1 i_1} + \omega_{\lambda_2 i_2} + \Delta\omega(\lambda_1 i_1, \lambda_2 i_2)) + 2\sum_{\lambda_1 i_1 \lambda_2 i_2 i} R_i(J\nu) P^{\lambda_1 i_1}_{\lambda_2 i_2}(J\nu) U^{\lambda_1 i_1}_{\lambda_2 i_2}(Ji)\left(1+\frac{1}{2}K^J(\lambda_2 i_2, \lambda_1 i_1 \mid \lambda_1 i_1, \lambda_2 i_2)\right), \quad (57)$$

where

$$\Delta\omega(\lambda_1 i_1, \lambda_2 i_2) = -\frac{1}{8}\sum_{i_3 \tau}\left[\frac{X^{\lambda_1 i_1}_M(\tau)+X^{\lambda_1 i_3}_M(\tau)}{\sqrt{y^{\lambda_1 i_1}_\tau y^{\lambda_1 i_3}_\tau}} K^J(\lambda_2 i_2, \lambda_1 i_3 \mid \lambda_1 i_1, \lambda_2 i_2) + \frac{X^{\lambda_2 i_2}_M(\tau)+X^{\lambda_2 i_3}_M(\tau)}{\sqrt{y^{\lambda_2 i_2}_\tau y^{\lambda_2 i_3}_\tau}} K^J(\lambda_2 i_3, \lambda_1 i_1 \mid \lambda_1 i_1, \lambda_2 i_2)\right], \quad (58)$$

the summation over i_3 being due to our going beyond the framework of the random-phase approximation.

We use the variational principle and obtain the system of equations

$$(\omega_{Ji} - \eta_\nu) R_i(J\nu) + \sum_{\lambda_1 i_1 \lambda_2 i_2} P^{\lambda_1 i_1}_{\lambda_2 i_2}(J\nu) U^{\lambda_1 i_1}_{\lambda_2 i_2}(Ji)\left\{1+\frac{1}{2}K^J(\lambda_2 i_2, \lambda_1 i_1 \mid \lambda_1 i_1, \lambda_2 i_2)\right\} = 0; \quad (59)$$

$$2(\omega_{\lambda_1 i_1} + \omega_{\lambda_2 i_2} + \Delta\omega(\lambda_1 i_1, \lambda_2 i_2) - \eta_\nu) P^{\lambda_1 i_1}_{\lambda_2 i_2}(J\nu) + \sum_i R_i(J\nu) U^{\lambda_1 i_1}_{\lambda_2 i_2}(Ji) = 0. \quad (60)$$

A secular equation can now be obtained both in the space of the two-phonon states and in the space of the single-phonon states. The secular equation in the first case has the form

$$\det\left\| (\omega_{\lambda_1 i_1} + \omega_{\lambda_2 i_2} + \Delta\omega(\lambda_1 i_1, \lambda_2 i_2) - \eta_\nu) \times (\delta_{\lambda_1 \lambda_1'}\delta_{i_1 i_1'}\delta_{\lambda_2 \lambda_2'}\delta_{i_2 i_2'} + \delta_{\lambda_1 \lambda_2'}\delta_{i_1 i_2'}\delta_{\lambda_2 \lambda_1'}\delta_{i_2 i_1'}) - \frac{1}{2}\sum_i \frac{U^{\lambda_1 i_1}_{\lambda_2 i_2}(Ji)\, U^{\lambda_1' i_1'}_{\lambda_2' i_2'}(Ji)}{\omega_{Ji} - \eta_\nu}\left(1+\frac{1}{2}K^J(\lambda_2 i_2, \lambda_1 i_1 \mid \lambda_1 i_1, \lambda_2 i_2)\right)\right\| = 0. \quad (61)$$

In this case, diagrams c, e, and h in Fig. 3 are taken into account, diagram h differing from diagram f in that there is no summation over intermediate two-phonon states, since only the diagonal value of K^J is retained, i.e., fewer diagrams are summed than in Eq. (55).

The secular equation in the space of single-phonon states has the form

$$\det\left\| (\omega_{Ji} - \eta_\nu)\delta_{ii'} - \frac{1}{2}\sum_{\lambda_1 i_1 \lambda_2 i_2} \frac{U^{\lambda_1 i_1}_{\lambda_2 i_2}(Ji)\, U^{\lambda_1 i_1}_{\lambda_2 i_2}(Ji')\left(1+\frac{1}{2}K^J(\lambda_2 i_2, \lambda_1 i_1 \mid \lambda_1 i_1, \lambda_2 i_2)\right)}{\omega_{\lambda_1 i_1} + \omega_{\lambda_2 i_2} + \Delta\omega(\lambda_1 i_1, \lambda_2 i_2) - \eta_\nu}\right\| = 0. \quad (62)$$

The diagrams in Fig. 4 are taken into account in the space of single-phonon states. As is shown in Ref. 39, numerical calculations of nuclear field theory need take into account only special cases of the diagram in Fig. 4a, when one of the intermediate phonons is replaced by a two-quasiparticle state and strongly collectivized phonons are taken as the other.

Consider Eq. (62). The rank of the determinant is equal to the number of single-phonon states in the first term of the wave function (47). The rank varies from 20 to 200 and is thus two orders of magnitude less than the rank of the determinants (55) and (61). The factor $[1+\frac{1}{2}K^J(\lambda_2 i_2, \lambda_1 i_1 \mid \lambda_1 i_1, \lambda_2 i_2)]$ is due to allowance for the Pauli principle in the two-phonon terms of the wave function (47). In the case of maximal violation of the Pauli principle $K^J = -2$, and the corresponding term is eliminated from the sum over $\lambda_1 i_1$ and $\lambda_2 i_2$. The shift $\Delta\omega(\lambda_1 i_1, \lambda_2 i_2)$ of the two-phonon pole is due to allowance for diagrams of the type in Fig. 3c. As is shown in Ref. 33, it is large for the first two-phonon collective states of deformed nuclei. The shift $\Delta\omega(\lambda_1 i_1, \lambda_2 i_2)$ is small for the collective phonons forming giant resonances of the various types. The shift $\Delta\omega(\lambda_1 i_1, \lambda_2 i_2)$ is equal to zero for $K^J = 0$. Using the normalization condition (56), we find

$$R_i^2(J\nu) = A_{ii}^2 \Big/ \left\{\sum_{i'} A_{ii'}^2 + \frac{1}{2}\sum_{\substack{\lambda_1 i_1 \\ \lambda_2 i_2}}\left[\frac{\sum_{i'} U^{\lambda_1 i_1}_{\lambda_2 i_2}(Ji') A_{ii'}}{\omega_{\lambda_1 i_1} + \omega_{\lambda_2 i_2} + \Delta\omega(\lambda_1 i_1, \lambda_2 i_2) - \eta_\nu}\right]^2 \times \left(1+\frac{1}{2}K^J(\lambda_2 i_2, \lambda_1 i_1 \mid \lambda_1 i_1, \lambda_2 i_2)\right)\right\}, \quad (63)$$

where $A_{ii'}$ is the cofactor of the determinant (62).

If in the commutation relation (17) we ignore the terms proportional to $\alpha^*\alpha$, then in this case $K^J = 0$ and instead of Eqs. (59) and (60) we have

$$(\omega_{Ji} - \eta_\nu) R_i(J\nu) + \sum_{\substack{\lambda_1 i_1 \\ \lambda_2 i_2}} U^{\lambda_1 i_1}_{\lambda_2 i_2}(Ji) P^{\lambda_1 i_1}_{\lambda_2 i_2}(J\nu) = 0; \quad (64)$$

$$P^{\lambda_1 i_1}_{\lambda_2 i_2}(J\nu) = -\frac{1}{2}\sum_{i'} \frac{U^{\lambda_1 i_1}_{\lambda_2 i_2}(Ji') R_{i'}(J\nu)}{\omega_{\lambda_1 i_1} + \omega_{\lambda_2 i_2} - \eta_\nu}. \quad (64')$$

We substitute the expression (64′) in (64) and obtain the

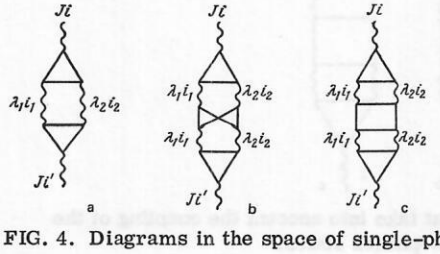

FIG. 4. Diagrams in the space of single-phonon states.

system of equations

$$\sum_{i'}\left[(\omega_{Ji}-\eta_\nu)\,\delta_{ii'}-\frac{1}{2}\sum_{\lambda_1 i_1\lambda_2 i_2}\frac{U^{\lambda_1 i_1}_{\lambda_2 i_2}(Ji)\,U^{\lambda_1 i_1}_{\lambda_2 i_2}(Ji')}{\omega_{\lambda_1 i_1}+\omega_{\lambda_2 i_2}-\eta_\nu}\right]R_{i'}(J\nu)=0. \quad (65)$$

From the condition of existence of a nontrivial solution of the system (65) we obtain a secular equation for determining the energies η_ν:

$$\mathscr{F}(\eta_\nu)=\det\left|(\omega_{Ji}-\eta_\nu)\,\delta_{ii'}-\frac{1}{2}\sum_{\lambda_1 i_1\lambda_2 i_2}\frac{U^{\lambda_1 i_1}_{\lambda_2 i_2}(Ji)\,U^{\lambda_1 i_1}_{\lambda_2 i_2}(Ji')}{\omega_{\lambda_1 i_1}+\omega_{\lambda_2 i_2}-\eta_\nu}\right|=0, \quad (65')$$

the rank of the determinant being equal to the number of single-phonon states in the wave function (47). Using the condition of normalization of the wave function (47) in the form

$$\sum_i (R_i(J\nu))^2+2\sum_{\lambda_1 i_1\lambda_2 i_2}(P^{\lambda_1 i_1}_{\lambda_2 i_2}(J\nu))^2=1, \quad (66)$$

we find

$$R_i^2(J\nu)=A_{ii}^2\Big/\left\{\sum_{i'}(A_{ii'})^2+\frac{1}{2}\sum_{\lambda_1 i_1\lambda_2 i_2}\left[\frac{\sum_{i'}A_{ii'}U^{\lambda_1 i_1}_{\lambda_2 i_2}(Ji')}{\omega_{\lambda_1 i_1}+\omega_{\lambda_2 i_2}-\eta_\nu}\right]^2\right., \quad (67)$$

where $A_{ii'}(\eta)=(-)^{i+i'}M_{ii'}(\eta)$; $M_{ii'}(\eta)$ is the corresponding minor of the determinant (65′). For the solutions of Eq. (65′) the following relations hold:

$$R_i^{-2}(J\nu)=-\left[\frac{1}{M_{ii}}\frac{\partial\mathscr{F}(\eta)}{\partial\eta}\right]\Big|_{\eta=\eta_\nu}; \quad (68)$$

$$R_i(J\nu)=\frac{(-)^{i+i'}M_{ii'}}{M_{ii}}R_{i'}(J\nu). \quad (68')$$

These properties of the coefficients R_i play a key role in the method of strength functions, which we shall consider somewhat later. The expressions (63)–(67) above were first obtained for deformed nuclei in Ref. 9, and for spherical nuclei in Ref. 10. In this case, we assume that the phonon operators are ideal bosons.

The charge-exchange states of odd–odd spherical nuclei can be described by wave functions of the form

$$\Psi_\nu(JM)=\left\{\sum_i R_i(J\nu)\,\Omega^+_{JMi}+\sum_{\lambda_1 i_1\lambda_2 i_2}P^{\lambda_1 i_1}_{\lambda_2 i_2}(J\nu)\,[\Omega^+_{\lambda_1\mu_1 i_1}Q^+_{\lambda_2\mu_2 i_2}]_{JM}\right\}\Psi_0 \quad (69)$$

with the normalization condition

$$\sum_i (R_i(J\nu))^2+\sum_{\lambda_1 i_1\lambda_2 i_2}(P^{\lambda_1 i_1}_{\lambda_2 i_2}(J\nu))^2=1. \quad (70)$$

We take the following part of the model Hamiltonian

$$H^C_M=\sum_{jm}\varepsilon_{jm}\alpha^+_{jm}\alpha_{jm}+H^{ph}_{Mvq}+H^{ph}_{Svq}+H^{ph}_{CMv}+H^{ph}_{CMvq} \quad (71)$$

and find the expectation value with respect to the wave function (69):

$$\begin{aligned}&\langle\Psi^*_\nu(JM)\,H^C_M\Psi_\nu(JM)\rangle\\&=\sum_i\Omega_{\lambda i}(R_i(J\nu))^2+\sum_{\lambda_1 i_1\lambda_2 i_2}(\Omega_{\lambda_1 i_1}+\omega_{\lambda_2 i_2})\,(P^{\lambda_1 i_1}_{\lambda_2 i_2}(J\nu))^2\\&\quad+2\sum_i\sum_{\substack{\lambda_1 i_1\\ \lambda_2 i_2}}V^{\lambda_1 i_1}_{\lambda_2 i_2}(Ji)\,R_i(J\nu)\,P^{\lambda_1 i_1}_{\lambda_2 i_2}(J\nu),\end{aligned} \quad (72)$$

where

$$V^{\lambda_1 i_1}_{\lambda_2 i_2}(Ji)=\langle|\,\Omega_{JMi}\,(H^{ph}_{Mvq}+H^{ph}_{CMvq})\,[\Omega^+_{\lambda_1\mu_1 i_1}Q^+_{\lambda_2\mu_2 i_2}]_{JM}\,|\rangle.$$

Using the variational principle, we obtain a secular equation for finding the energies η_ν of the states (69) in the form

$$\mathscr{F}(\eta_\nu)=\det\left|(\Omega_{Ji}-\eta_\nu)\,\delta_{ii'}-\sum_{\substack{\lambda_1 i_1\\ \lambda_2 i_2}}\frac{V^{\lambda_1 i_1}_{\lambda_2 i_2}(Ji)\,V^{\lambda_1 i_1}_{\lambda_2 i_2}(Ji')}{\Omega_{\lambda_1 i_1}+\omega_{\lambda_2 i_2}-\eta_\nu}\right|=0. \quad (73)$$

As in the case of multipole phonons, we obtain

$$P^{\lambda_1 i_1}_{\lambda_2 i_2}(J\nu)=-\frac{\sum_i R_i(J\nu)\,V^{\lambda_1 i_1}_{\lambda_2 i_2}(Ji)}{\Omega_{\lambda_1 i_1}+\omega_{\lambda_2 i_2}-\eta_\nu}. \quad (74)$$

For the coefficients $R_i(J\nu)$ the relation (68) still holds if instead of (65) we use (73) and its corresponding minor.

3. THE METHOD OF STRENGTH FUNCTIONS AND DETAILS OF CALCULATION

As the excitation energy increases, there is a rapid increase in the density of the levels, the structure of the wave functions becoming more complicated. Much of the experimental information about highly excited states is represented in the form of quantities averaged or summed in definite energy intervals. Therefore, instead of solving equations of the type (64) and (64′), which is a complicated computational problem, one should instead directly calculate the distribution of the physical quantities in the chosen interval of excitation energies. The procedure of averaging over the energy has been widely used in the statistical description of nuclear reactions.[36]

We shall be interested in the distribution of physical quantities due to fragmentation of single-phonon states. Because of the quasiparticle–phonon interaction, the single-phonon states are coupled directly only to the two-phonon states, and therefore the use of the wave function (47) in calculations makes it possible to obtain a correct description of the distribution of the strength of the single-phonon states. The problem of calculating the energy-averaged characteristics can be solved by using the method of strength functions developed in the quasiparticle–phonon model of the nucleus.[14-29] A simple example of the use of the method is given in Ref. 37. Recently, it has also been used in other studies.[38-42]

We shall explain the method. Let $\Phi_{J\nu}$ be the amplitude for excitation of the state $\Psi_\nu(JM)$ in some physical process. We define the strength function as follows:

$$b(\Phi,\eta)=\sum_\nu\rho(\eta-\eta_\nu)\,|\,\Phi_{J\nu}\,|^2, \quad (75)$$

where we have chosen the weight function $\rho(\eta-\eta_\nu)$, which is normalized to unity, in the form

$$\rho(\eta-\eta_\nu)=\frac{1}{2\pi}\frac{\Delta}{(\eta-\eta_\nu)^2+\Delta^2/4}. \quad (76)$$

If the excitation of the state $\Psi_\nu(JM)$ occurs through single-phonon components of the wave function (47), then

$$\Phi_{J\nu}=\sum_i R_i(J\nu)\,\Phi_{Ji}. \quad (77)$$

Substituting (77) in (75) and using the relations (68) and (68′), we rewrite (75) in the form

$$\begin{aligned}b(\Phi,\eta)&=\sum_\nu\rho(\eta-\eta_\nu)\sum_{ij}\frac{A_{ij}}{A_{jj}}R_i^2\Phi_{Ji}\Phi_{Jj}\\&=\sum_\nu\rho(\eta-\eta_\nu)\,\Phi^2(\eta_\nu)\Big/\left(\frac{\partial\mathscr{F}}{\partial\eta}\right)\Big|_{\eta=\eta_\nu},\end{aligned} \quad (78)$$

where $\Phi^2(\eta_\nu)=-\sum_{ij}A_{ij}(\eta_\nu)\Phi_{Ji}\Phi_{Jj}$.

We go over to the integral

$$b(\Phi,\eta)=\frac{1}{2\pi i}\oint_{C_z}\frac{\Phi^2(z)}{\mathscr{F}(z)}\rho(\eta-z)\,dz \quad (79)$$

around a contour (see Fig. 2 in Ref. 14) C_z, which surrounds the poles $z=\eta_\nu$ of the integrand $\mathscr{F}^{-1}(z)$, these being roots of the secular equation (65′). Expressing (79) in terms of an integral around an infinitely distant con-

tour (which vanishes, since the integrand decreases at infinity as $|z|^{-3}$) and integrating around contours surrounding the poles of the function $\rho(\eta - z)$, which are at $z = \eta \pm i\Delta/2$, and using the residue theorem, we obtain

$$b(\Phi, \eta) = \frac{1}{\pi} \operatorname{Im} \left\{ \frac{\sum_{ij} A_{ij} \left(\eta + i\frac{\Delta}{2}\right) \Phi_{Ji} \Phi_{Jj}}{\mathcal{F}\left(\eta + i\frac{\Delta}{2}\right)} \right\}, \quad (80)$$

where $\mathcal{F}(\eta + i\Delta/2)$ is the determinant (65′) for complex values of the energy, and A_{ij} are its cofactors. Thus, to find the average characteristics it is not necessary to solve secular equations; instead, one calculates determinants for complex energies, which is much simpler. The energy interval Δ of the averaging determines the method of representing the results of the calculations. In the limit $\Delta \to 0$, the Lorentz function $\rho(\eta - \eta_\nu)$ goes over into the Dirac δ function, and the strength function $b(\Phi, \eta)$ is nonzero only at the points $\eta = \eta_\nu$ of the solution of Eq. (65′) and is equal to $|\Phi_{J\nu}|^2$. The interval of averaging Δ must be greater than the average distance between the states corresponding to the many-phonon components ignored in (47). In addition, Δ must be appreciably less than the region of localization of the calculated physical quantity. In spherical nuclei, these criteria are satisfied for $0.1 \leq \Delta \leq 1$ MeV. In Ref. 16, the dependence of the strength functions on the choice of the form of $\rho(\eta - \eta_\nu)$ was studied, and it was shown that in the majority of cases different forms of ρ give similar results. We note also that in the limit $\Delta \to 0$ it is possible to establish a unique connection between the strength functions and the response functions of the nucleus to an external perturbation (see Ref. 38).

Since a detailed description of the procedure for choosing the constants in the quasiparticle–phonon model is given in the review of Ref. 17, we shall merely mention them briefly. In numerical calculations, the parameters of the Woods–Saxon potential are taken to be the same as in Refs. 17 and 43. The constants of the monopole pairing are chosen on the basis of the experimental values of the pairing energies. The constants of the multipole and spin-multipole forces are determined on the basis of the experimental data on the energies and probabilities of electromagnetic transitions of low-lying levels. For this, the wave functions (47) are used. More detailed information about the constants can be found in the original papers cited below. All calculations with the wave function (47) are made with the program GIRES.[32]

The possibility of simultaneous description of low-lying and highly excited states with a common set of parameters was demonstrated in Ref. 44 for the example of ^{208}Pb. The results of calculations of the characteristics of ^{208}Pb in the quasiparticle–phonon model agree well with the experimental data of Ref. 45 and other theoretical calculations.[46-50]

4. FRAGMENTATION OF SINGLE-PHONON STATES

One of the processes in which fragmentation of the single-phonon states is clearly manifested is the photoexcitation of giant multipole resonances. Extensive experimental information on such resonances has been accumulated (see Refs. 51–54), and it is steadily being augmented by new data. A large body of experimental data on the best studied giant electric dipole resonance is given in Ref. 54.

In the case of excitation of the state $\Psi_\nu(JM)$ by γ rays, the expression for Φ_{Ji} in Eq. (80) has the form

$$\Phi_{Ji} = \langle \Psi_0 \| M(EJ(MJ)) Q^+_{JMi} \| \Psi_0 \rangle, \quad (81)$$

where $M[EJ(MJ)]$ is the operator of the electric (magnetic) transition of multipolarity J. For example, for $E\lambda$ transitions

$$\Phi_{Ji} = \left[e^{(J)} \frac{X^{Ji}_M(n)}{\sqrt{\mathscr{y}^{Ji}_n}} + (1 + e^{(J)}) \frac{X^{Ji}_M(p)}{\sqrt{\mathscr{y}^{Ji}_p}} \right] e. \quad (82)$$

Here, $e^{(J)}$ is the effective charge, and $e^{(1)} = -z/A$, $e^{(J)} = 0$ for $J \geq 2$; e is the electron charge; X^{Ji}_M and $\mathscr{y}^{Ji}_\tau$ are defined in (28) and (30). In deriving (82), we ignored the terms proportional to $\alpha^+\alpha$ in the operator of the $E\lambda$ transition (see Ref. 4) and used the radial dependence $R(r) = r^\lambda$ of the forces. Substituting (82) in (80), we obtain the strength function, by means of which we can calculate the distribution of the strength of the electromagnetic transitions at different excitation energies.

To analyze giant multipole resonances, energy-weighted sum rules are used. The model-independent dipole energy-weighted sum rule has the form

$$S^{\lambda=1}_\Delta = \sum_{\nu \in \Delta} b(E1, \eta_\nu) \eta_\nu = \frac{9}{8\pi} \frac{e^2\hbar^2}{m} \frac{Nz}{A} = 0.18 \frac{Nz}{A}. \quad (83)$$

For resonances of multipolarity $\lambda \geq 2$

$$S^\lambda_\Delta = \sum_{\nu \in \Delta} b(E\lambda, \eta_\nu) \eta_\nu = 1.65\lambda (2\lambda + 1)^2 z \langle r^{2\lambda-2} \rangle$$
$$= 4.95\lambda (2\lambda + 1) (1.2)^{2\lambda-2} z A^{\frac{2\lambda-2}{3}} \cdot 10^{-2\lambda}. \quad (84)$$

In (84), $\langle r^{2\lambda-2} \rangle$ is estimated for a rectangular well with radius $1.2A^{1/3}$ F. For the isoscalar part of (84), we have

$$\sum_\nu b(E\lambda, \eta_\nu) \eta_\nu = 4.95\lambda (2\lambda + 1) (1.2)^{2\lambda-2} z^2 A^{\frac{2\lambda-5}{3}} \cdot 10^{-2\lambda}. \quad (85)$$

All the S^λ_Δ are given in units of $e^2 \cdot b^\lambda \cdot$ MeV.

We begin our discussion with the giant dipole resonance. Figure 5, which is taken from Ref. 55, shows the distribution of the probabilities of $E1$ transitions in ^{90}Zr, calculated in the RPA (Fig. 5a) and with the wave function (47) (Fig. 5b) and $\Delta = 1$ keV. For Δ with this small value, $\int_\Delta b(E1, \eta) d\eta = B(E1, 0^+_{gs} \to 1^-_\nu)$, and the results of the calculations of the $B(E1)$ values with the wave functions (47) are reproduced without the use of the method of strength functions. It can be seen from Fig. 5 that allowance for the two-phonon components leads to strong fragmentation of the dipole strength. The calculations in Ref. 22 of the energy-weighted sum rules for dipole transitions in ^{90}Zr, ^{120}Sn, and ^{124}Te exhaust 90–95% of the model-independent energy-weighted sum rule (83) and agree well with the experimental data of Refs. 54 and 56. This indicates that the configuration space used in the calculations is complete.

Much information about the integrated characteristics of the giant dipole resonances is obtained from the photoabsorption cross sections.[54] The cross section of dipole photoabsorption (mb) is related to the strength

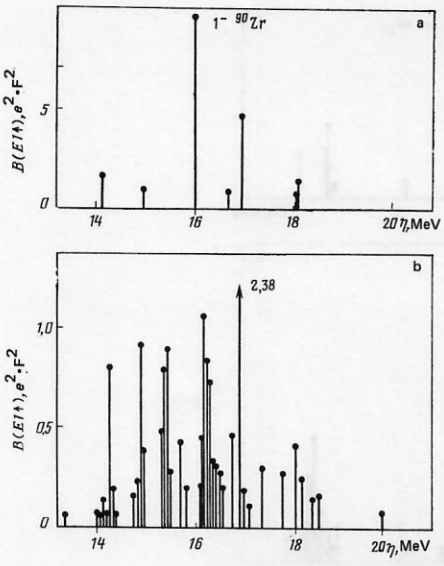

FIG. 5. Calculated values of $B(E1)$ ($e^2 \cdot F^2$) in ^{90}Zr: a) in the single-phonon approximation; b) with allowance for the quasiparticle–phonon interaction.

function $b(E1, \eta)$ by[24]

$$\sigma_{\gamma t}(E) = (4.025E/\Delta) \int_{E-\frac{1}{2}\Delta}^{E+\frac{1}{2}\Delta} b(E1, \eta)\, d\eta. \quad (86)$$

Here, E is the energy of the γ transition in MeV, and $b(E1, \eta)$ is measured in units of $e^2 \cdot F^2$/MeV. For the integrated cross sections,[57] we have

$$\sigma_0 = \int_{B_n}^{E_u} \sigma_{\gamma t}(E)\, dE; \quad (87)$$

$$\sigma_{-1} = \int_{B_n}^{E_u} E^{-1}\sigma_{\gamma t}(E)\, dE; \quad (88)$$

$$\sigma_{-2} = \int_{B_n}^{E_u} E^{-2}\sigma_{\gamma t}(E)\, dE, \quad (89)$$

where E_u is the upper limit of integration, and B_n is the neutron separation energy.

The results of our calculations[24] of $\sigma_{\gamma t}$ with $\Delta = 0.4$ MeV for ^{124}Te, $^{140,142}Ce$ and the experimental data of Ref. 57 are shown in Figs. 6–8. As can be seen from these figures, a qualitatively correct description of the total photoabsorption cross sections is obtained. In the calculations, the central peak is higher than the experimental peak, and the fine structure of the giant dipole resonance is expressed more clearly than in the experimental cross sections. This is evidently due to the fact that we ignore the more complicated configurations in our wave functions. We note that the use of the microscopic approach makes it possible to take into account in a natural manner individual properties of individual nuclei. For example, the width of the giant dipole resonance in ^{142}Ce is appreciably greater than in ^{140}Ce. As can be seen from Figs. 7 and 8, our calculations correctly describe the decrease of the peak in $\sigma_{\gamma t}$ and the broadening of the giant resonance in ^{142}Ce compared with ^{140}Ce. The anharmonic effects, which basically determine the widths of the giant dipole resonances, are enhanced on the transition from the semimagic nucleus ^{140}Ce to the nonmagic ^{142}Ce.

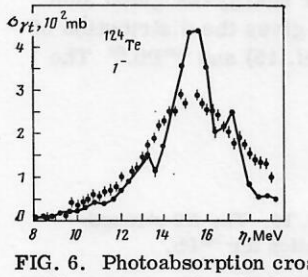

FIG. 6. Photoabsorption cross section $\sigma_{\gamma t}$ for ^{124}Te. The continuous curve is calculated with $\Delta = 0.4$ MeV; the points are the experimental data of Ref. 57.

The experimental data of Refs. 57 and 58 and the results of our calculations[24,59] of the integrated cross sections of dipole photoabsorption are given in Table I. It can be seen that our calculations give for the integrated characteristics of the giant dipole resonance values close to the experimental ones and correctly describe their variation on the transition from one nucleus to another.

The giant quadrupole resonance has been studied less than the dipole resonance, but its existence is firmly established.[52] According to the systematization of the experimental data on the excitation of the isoscalar giant quadrupole resonance in nuclei with $40 \leqslant A \leqslant 208$, its energy is $E \sim 63A^{-1/3}$ MeV, and 50–100% of the isoscalar energy-weighted sum rule is exhausted. Information about the isovector giant quadrupole resonance in nuclei with $A \geqslant 60$ is sparse. The known energies of isovector giant quadrupole resonances agree with $E \sim 110A^{-1/3}$ MeV.

The distribution of the strengths of the quadrupole excitations in ^{90}Zr is shown in Fig. 9. It can be seen from the figure that there undoubtedly is fragmentation (especially for the isovector giant quadrupole resonance). However, in ^{208}Pb, for example, in which RPA calculations[60] give one collective state with excitation energy 10.1 MeV, this exhausting 72% of the isoscalar energy-weighted sum rule [see Eq. (85)], allowance for the two-phonon components leads to a radical redistribution of the strength of the isoscalar giant quadrupole resonance. This can be seen in Fig. 10, which shows the strength function $b(E2, \eta)$ for ^{208}Pb. The individual properties of the nuclei determine how the strength is distributed.

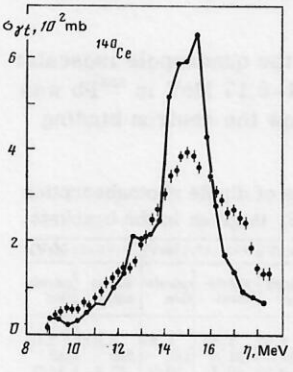

FIG. 7. Photoabsorption cross sections $\sigma_{\gamma t}$ for ^{140}Ce. The notation is the same as in Fig. 6.

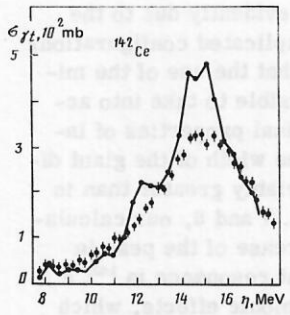

FIG. 8. Photoabsorption cross sections $\sigma_{\gamma t}$ for ^{142}Ce. The notation is the same as in Fig. 6.

The results of calculations[24,60] and experimental data for the energies in the energy-weighted sum rule of the isoscalar giant quadrupole resonance in various nuclei are given in Table II. The experimental data from different reactions give a spread for the energy of the resonance over 1 MeV. The extent to which the energy-weighted sum rule is exhausted differs strongly.

Our calculations of the distribution of the $E2$ strength in ^{208}Pb show that the major part of it (66% of the energy-weighted sum rule) is concentrated in the interval 8–11 MeV with centroid at $\overline{E}$ = 9.5 MeV. Substructures are observed in the resonance at the energies 8.8, 9.5, 10.4, and 10.8 MeV. According to Refs. 64 and 65, which report excitation of the isoscalar giant quadrupole resonance in the (α, α') and (d, d') reactions on ^{208}Pb, $\overline{E}$ = 10.5–10.9 MeV and the energy-weighted sum rule is exhausted to 60–80%. A fine structure of the resonance is observed experimentally. A large number of individual 2^+ states are found in the interval of excitation energies 8–12 MeV in electron scattering on ^{208}Pb.[66] There is a certain grouping of the states at the energies 8.9, 10.2, and 10.6 MeV and, possibly, at 11.2 MeV. Qualitatively, the experimental data on the fragmentation of the $E2$ strength are very similar to what we calculate. However, from electron scattering only (29^{+11}_{-8})% of the energy-weighted sum rule is obtained. The calculations made in Ref. 66 in accordance with the MSI model[67] with allowance for $(2p-2h)$ configurations give $\overline{E} \approx 9.6$ MeV, and about 30% of the energy-weighted sum rule is exhausted. However, 45% of the $E2$ strength is displaced into the interval 12–20 MeV and is distributed over a large number of weakly excited states. Neither our calculations nor the data of Refs. 39–41 with allowance for $(2p-2h)$ configurations give such strong fragmentation of the $E2$ strength.

In Ref. 68, the distribution of the quadrupole isoscalar strength in the energy interval 4–8.17 MeV in ^{208}Pb was measured. For states lying below the neutron binding energy without allowance for the 2^+_1 level, the sum of the reduced probabilities of the $E2$ transitions is $\Sigma B(E2) = 480\ e^2 \cdot F^4$. Our calculations give $\Sigma B(E2) = 465\ e^2 \cdot F^4$. The experiment of Ref. 68 also revealed a group of states with appreciable $B(E2)$ values at energies 7.8–8.2 MeV with $\Sigma B(E2) = 541\ e^2 \cdot F^4$. Our calculations give a certain concentration of the $E2$ strength in this interval, and we obtain $\Sigma B(E2) = 240\ e^2 \cdot F^4$. To within the experimental values, we obtain the correct distribution of the strength of the quadrupole excitations in a wide interval of energies.

TABLE I. Integrated cross sections of dipole photoabsorption for different nuclei. The value of E_u is given in the brackets.

Cross section	^{124}Te (19 MeV)		^{140}Ce (18.5 MeV)		^{142}Ce (17.4 MeV)		^{208}Pb (25 MeV)	
	experiment	calculation	experiment	calculation	experiment	calculation	experiment	calculation
σ_0, b·MeV	1.46	1.5	1.77	1.9	1.89	1.96	3.059	2.88
σ_{-1}, mb	98.7	102.9	123	137	131.8	142	229	213
σ_{-2}, mb · MeV^{-1}	6.6	7.0	8.8	9.8	10.2	10.5	17.6	16.2
E_{GDR}, MeV	15.2	15.5	15.0	15.2	14.9	15.1	13.43	13.4

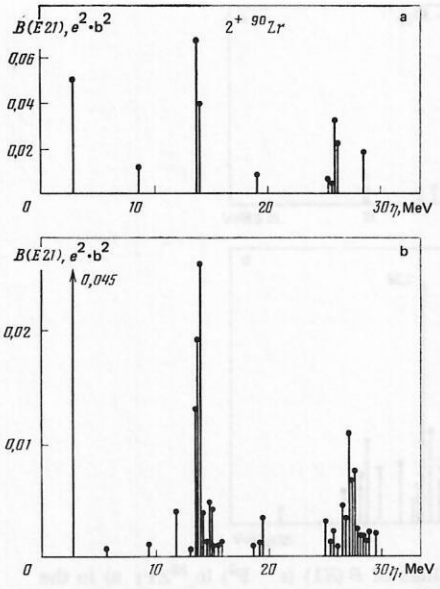

FIG. 9. Calculated values of $B(E2\uparrow)$ in ^{90}Zr: a) in the single-phonon approximation; b) with allowance for the quasiparticle–phonon interaction.

For the isovector giant quadrupole resonance, our calculations[44] for ^{208}Pb give $\overline{E}$ = 21.3 MeV, and about 70% of the isovector energy-weighted sum rule is exhausted. According to the experimental data,[64] $\overline{E}$ = 21.5 MeV, and 80% of the sum rule is exhausted.

The distribution of the octupole strength in spherical nuclei has been studied experimentally even less. From simple considerations based on nuclear shell structure one can expect the existence of an isoscalar low-energy octupole resonance, corresponding to transitions through one shell, and a high-energy octupole isoscalar resonance associated with transitions through three shells. The low-energy resonance was discovered in inelastic scattering of α particles in many spherical nuclei.[65,69] It is at energies 4.5–7 MeV and exhausts between 8 and 20% of the isoscalar energy-weighted sum rule. As an example, Table III gives the distribution of the octupole strength in ^{58}Ni (Ref. 15) and ^{208}Pb.[60] The

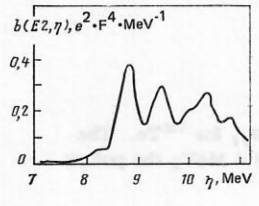

FIG. 10. The $E2$ strength function for ^{208}Pb.

TABLE II. Energies and the extent to which the model-independent energy-weighted sum rule is exhausted for the isoscalar giant quadrupole resonance.

Nucleus	Experiment			Theory	
	E_x, MeV	EWSR, %	Reference	E_x, MeV	EWSR, %
^{90}Zr	14.0±0.3 14.0±0.2 14.1	40 68 65	[61] [62] [63]	14,0	45
^{120}Sn	12.8±0.3 13.3	46 70	[61] [63]	12.6	59
^{208}Pb	10.9 10.5	73 60	[63] [64]	9.5	66

experimental data for ^{58}Ni are taken from Ref. 69. The calculations describe well the 3_1^- level and the low-energy octupole resonance in ^{58}Ni. Moreover, as is shown in Ref. 15, allowance for the two-phonon components in ^{58}Ni is basically important for this. Recently, experimental data have been obtained from α-particle scattering on ^{208}Pb for the low-energy[70] and high-energy[65] resonances. In Ref. 70, four 3^- levels were observed in the energy interval 4.5–5.7 MeV. Our calculations for the low-energy octupole resonance give good agreement with the experiment for the level energies, and an exhaustion of the energy-weighted sum rule that is approximately 1.8 times smaller. The results of our calculations for the high-energy resonance are in good agreement with the experimental data.[65] From neutron scattering on ^{208}Pb it is found[64] that for the high-energy octupole isoscalar resonance $\overline{E}$ = 17.8 MeV and only 12% of the energy-weighted sum rule is exhausted. This small percentage contradicts the data of Ref. 65 and our calculations. The investigations of Ref. 24 of the low-energy octupole resonance in ^{90}Zr and ^{120}Sn also agree well with the available experimental data.[69]

The giant multipole resonances are excited differently in different reactions. To understand the excitation mechanism of the structure of the resonances, it is important to analyze the different processes in the framework of a unified theoretical approach. In part, this program has been realized in the quasiparticle–phonon model.[71,72] For example, in Ref. 71 calculations are made of the squares of the form factors of inelastic electron scattering with excitation of giant dipole and quadrupole resonances in ^{90}Zr as functions of the effective momentum transfer q_{eff}, which is widely used to analyze experimental data (Fig. 11).[73] The calculations reproduce the experimental data well.[73] The square of the form factor for the lowest 2^+ level in ^{90}Zr is described simultaneously with the same parameters (Fig. 12). The experimental points are taken from Ref. 74. Scattering of high-energy protons with excitation of the giant quadrupole resonance was investigated for a number of spherical nuclei in Ref. 72, in which it was shown that the isoscalar giant quadrupole resonance is well excited in the case of the scattering of high-energy hadrons.

Thus, in the quasiparticle–phonon model one can describe the characteristics of the giant multipole resonances and investigate their excitation mechanisms.

One further source of information about the fragmentation of the single-phonon components of the wave functions is the radiative strength functions. The best studied are the $E1$ and $M1$ strength functions. The radiative strength functions and the influence on them of giant dipole resonances have been analyzed in a number of reviews.[76–80] Here, we shall restrict ourselves to considering $E\lambda$ transitions, since magnetic giant resonances and the radiative strength functions of $M\lambda$ transitions warrant a separate description. The radiative strength functions are equal to

$$\langle k(E\lambda)\rangle = \sum_{\nu\in\Delta E} \Gamma_{\gamma 0}(E\lambda, \eta_\nu)/E_\gamma^{2\lambda+1} A^{2/3\lambda}\Delta E, \qquad (90)$$

where $\Gamma_{\gamma 0}$ (eV) are the partial widths of the γ transitions from the states $\Psi_\nu(JM)$ to the ground states, E_γ is the mean transition energy, and ΔE is the interval of averaging about the energy E_γ. We can express $\Gamma_{\gamma 0}$ in terms of the strength functions defined by Eqs. (80) and (81) (Refs. 23–25):

$$\sum_{\nu\in\Delta E} \Gamma_{\gamma 0}(E1, \eta_\nu) = 0.35 \int_{E-\frac{1}{2}\Delta E}^{E+\frac{1}{2}\Delta E} \eta^3 b(E1, \eta)\, d\eta; \qquad (91)$$

$$\sum_{\nu\in\Delta E} \Gamma_{\gamma 0}(E2, \eta_\nu) = 1.61\cdot 10^{-7} \int_{E-\frac{1}{2}\Delta E}^{E+\frac{1}{2}\Delta E} \eta^5 b(E2, \eta)\, d\eta. \qquad (92)$$

In these expressions, $b(E\lambda, \eta)$ is measured in the units $e^2 \cdot F^{2\lambda} \cdot MeV^{-1}$ and η in MeV. The major part of the experimental data on the radiative strength functions has been obtained for excitation energies in the region of the neutron binding energy B_n. The radiative strength functions are calculated in Refs. 23–25, 28, and 81.

TABLE III. Distribution of the octupole strength in ^{58}Ni and ^{208}Pb.

States	^{58}Ni				^{208}Pb			
	E_x, MeV		EWSR, %		E_x, MeV		EWSR,%.	
	experiment	theory	experiment	theory	experiment	theory	experiment	theory
3_1^-	4,47	4.35	10,0	8.4	2.61	2.4	20	21.3
Low-energy octupole resonance	6.9	7.5	8,0	7.2	4.7 4.96 5.34 5.58	4.8 5.0 5.3 5.8	1.5 1.6 2.5 7.1	0.93 0.3 2.61 3.82
High-energy octupole resonance	—	—	—	—	17.5	17.4	60	58.3

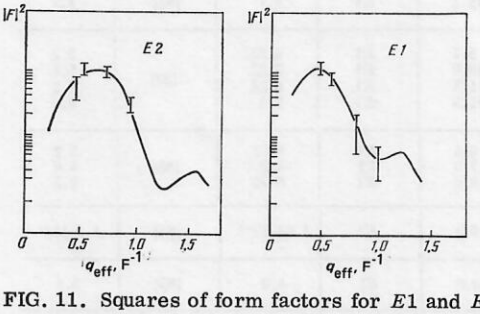

FIG. 11. Squares of form factors for $E1$ and $E2$ resonances calculated with allowance for the quasiparticle–phonon interaction. The points are the experimental data of Ref. 73.

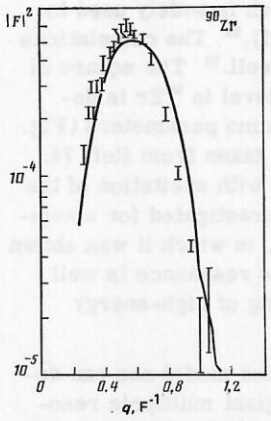

FIG. 12. Square of the form factor of the lowest 2^+ level in ^{90}Zr. The experimental data are taken from Ref. 74.

The results of the calculations of Refs. 23 and 24 and the experimental data[82-86] for the $E1$ strength functions are given in Table IV. The calculated values of $\langle k(E1)\rangle$ differ from the corresponding experimental values by not more than two times. It should be emphasized that in these calculations there are no free parameters, since they are fixed in the calculations of the low-lying states and the giant dipole resonance. Therefore, our distributions of the dipole strength indicate that the model correctly reflects the nuclear dynamics.

We shall discuss the influence of the giant dipole resonance on the $E1$ strength functions. In the analysis of the $E1$ strength functions, one frequently uses the Brink–Axel treatment, in accordance with which the dependence of the dipole photoabsorption cross sections on the energy of the γ rays is determined by Lorentz extrapolation of the giant dipole resonance to the low-energy region. In this case, the photoabsorption cross section has the form

$$\sigma_{\gamma l}(E) = \sigma_0 \frac{\Gamma_0^2 E^2}{(E^2 - E_0^2)^2 + E^2\Gamma_0^2}, \qquad (93)$$

where E_0 is the energy and Γ_0 is the width of the giant dipole resonance. It is assumed that a Lorentz shape reproduces the energy dependence reasonably well in nuclei that are far from magic. However, Lorentz extrapolation of the giant dipole resonance gives overestimated values of the $E1$ strength functions in the neighborhood of B_n for nuclei with nearly closed shells. Indeed, for ^{138}Ba the experimental value is $\langle k(E1)\rangle = 4\times10^{-9}$, whereas $\langle k(E1)\rangle = 9\times10^{-9}$ according to (93). In ^{140}Ce, the experimental value is $\langle k(E1)\rangle = 2.2\times10^{-9}$, while (93) gives $\langle k(E1)\rangle = 9.8\times10^{-9}$.

TABLE IV. The $E\lambda$ radiative strength functions.

Nucleus	E_γ, MeV	$E\lambda$	$\langle K(E\lambda)\rangle$, 10^{-9} MeV$^{-(2\lambda+1)}$		
			experiment	reference	calculation
^{56}Fe	11.2	$E1$	1.7	[82]	1.7
^{90}Zr	8.7 10.0 11.3 11.9	$E1$ $E1$ $E1$ $E1$	3.25 3.25 6.24 7.1	[83]	2.2 5.1 7.2 9.6
Sn	6.4 7.0 8.6	$E1$ $E1$ $E1$	5.02 4.2 8.35	[83]	3.2 4.6 9.5
^{136}Ba	9.1	$E2$	$1.02\cdot10^{-4}$	[84]	$1.2\cdot10^{-4}$
^{138}Ba	8.6	$E1$	4.0	[85]	3.9
^{140}Ce	9.08	$E1$	2.2	[86]	2.1

We shall study the influence of the giant dipole resonance on the behavior of the radiative strength functions $b(E1,\eta)$ in the energy interval 6–10 MeV. First, we calculate $b(E1,\eta)$ with the wave function (47), in whose single-phonon part we include only the RPA solutions lying in the interval 6–10 MeV. In this case, the functions $b(E1,\eta)$ are determined by the fragmentation of the single-phonon states with energy lying in the considered energy interval. The results of these calculations, in which the giant dipole resonance was not taken into account, are shown in Figs. 13 and 14 for ^{124}Te and ^{146}Nd. Further, we calculate $b(E1,\eta)$ in the same energy intervals with the wave function (47), in whose single-phonon part we include in addition to the previously considered RPA solutions the single-phonon states that form the giant dipole resonance (Figs. 13 and 14). The difference between the behavior of the functions $b(E1,\eta)$ calculated with and without allowance for the giant dipole resonance determine its influence on the $E1$ radiative strength functions. It can be seen from the figures that the resonance has a large influence on the $E1$ strength functions, its influence increasing with increasing excitation energy. The function $b(E1,\eta)$ behaves nonmonotonically as a function of the energy. These substructures are due to nearby single-phonon states and the displacement of some of the strength of the giant dipole resonance to this energy region.

The influence of the giant dipole resonance on the radiative strength functions for many nuclei was investigated by calculating $S^{\lambda=1}_{\Delta E}$ [see Eq. (83)] in the energy interval ΔE with and without allowance for the resonance. The results of the calculations are given in Table V. The function $S^{\lambda=1}_{\Delta E}(0)$ is calculated with single-phonon states in the interval ΔE. The function $S^{\lambda=1}_{\Delta E}$(GDR) is calculated with additional allowance for the phonons that form the giant dipole resonance. It can be seen from Table V that in ^{90}Zr and ^{118}Sn the influence of the giant dipole resonance on $b(E1,\eta)$ is small. Its influence is also small in the other ten isotopes. In ^{90}Zr, an appreciable increase in $S^{\lambda}_{\Delta E}(0)$ in the interval 8–10 MeV occurs if allowance is made for the single-phonon

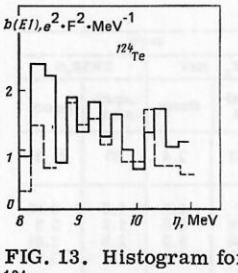

FIG. 13. Histogram for the strength function $b(E1,\eta)$ in ^{124}Te. The continuous line is the result of calculation with allowance for the giant dipole resonance; the broken line, without allowance for it.

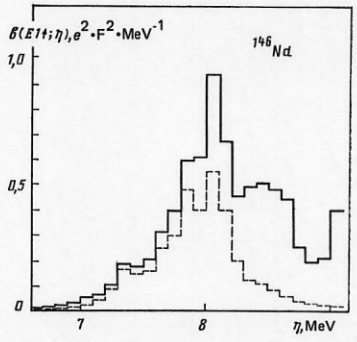

FIG. 14. Histogram for the strength function $b(E1, \eta)$ in ^{146}Nd. The notation is the same as in Fig. 13.

states lying above 10 MeV and below the giant dipole resonance. If the function $b(E1, \eta)$ is represented in the form of histograms of the type of Fig. 13 for the ten isotopes, then the lines in the cases with and without allowance for the giant dipole resonance almost coincide. The influence of the giant dipole resonance on the radiative strength functions is small in the semimagic nuclei ^{138}Ba, ^{140}Ce, and ^{142}Ce. On the basis of our calculations, we can conclude that the influence of the giant dipole resonance on the functions $b(E1, \eta)$ in the region of the neutron binding energy is small in semimagic nuclei. In these nuclei, the functions $b(E1, \eta)$ are to a large degree determined by the fragmentation of the single-phonon states lying near B_n. With increasing distance from closed shells, the influence of the giant dipole resonance on $b(E_1, \eta)$ increases, as is demonstrated in Table V. Thus, in ^{144,146}Nd the function $S_{\Delta E}$(GDR) is more than twice $S_{\Delta E}(0)$. The influence of the resonance does not reduce to a general raising of the function $b(E1, \eta)$. There is a redistribution of the dipole strength and a raising of the local maxima. As a result, the function $b(E1, \eta)$ becomes more strongly nonmonotonic in its dependence on the excitation energy.

It should be noted that in the calculation of the functions $b(E1, \eta)$ in the energy interval ΔE it is necessary to take into account the RPA solutions lying in this interval ΔE even if they make a small contribution to $b(E1, \eta)$ and to $S_{\Delta E}$. Such single-phonon terms in the wave function (47) must also be taken into account when the influence of the giant dipole resonance on $b(E1, \eta)$ is large. This is due to the fact that RPA solutions that make a small contribution to $b(E1, \eta)$ have a strong influence on the behavior of $b(E1, \eta)$ in the energy region in which they are situated. In a number of cases, weak single-phonon states hinder the penetration of the strengths of the giant dipole resonance into the energy region in which these solutions are situated.

Irregularities in the energy dependence of $b(E1, \eta)$ must be manifested in the photoexcitation cross sections $\sigma_{\gamma t}$. We shall study the dependence of the cross section $\sigma_{\gamma t}$ on the excitation energy and compare it with the behavior of a Lorentz curve. The calculated[24] and measured[83] cross sections $\sigma_{\gamma t}$ for ^{90}Zr are given in Fig. 15, from which it can be seen that the general behavior of the cross section follows a Lorentz curve. The dependence of the cross sections on the excitation energy exhibits irregularities, but they are not strongly expressed.

Appreciable substructures are observed in $\sigma_{\gamma t}$ for ^{140}Ce. The results of the calculation of the cross section $\sigma_{\gamma t}$ for ^{140}Ce and the experimental data obtained in Ref. 87 for natural cerium are shown in Fig. 16. Since natural cerium contains 89% of ^{140}Ce, a detailed comparison of theory with experiment can be made. In the measured cross section $\sigma_{\gamma t}$ a maximum is observed at energy 7.8 MeV; in the calculated cross section, there is a higher maximum at 8 MeV. In our calculations in semimagic nuclei, the fragmentation of the single-phonon states is much weaker than in nuclei far from closed shells. The appearance of the large peak at 8 MeV is due to this circumstance. The calculations correctly reproduce the raising of the cross sections at

TABLE V. Influence of the giant dipole resonance on the function $S_{\Delta E}^{\lambda=1}$.

Nucleus	Number of single-phonon components in Eq. (47)	Energy interval, MeV, in which the single-phonon component lie	Energy interval ΔE, MeV	$S_{\Delta E}^{\lambda=1}$, $e^2 \cdot F^2 \cdot$MeV	$\frac{S_{\Delta E}^{\lambda=1}\text{(GDR)}}{S_{\Delta E}^{\lambda=1}(0)}$
^{90}Zr	9 10	8—13 8—16	8—13	9.43 11.2	1.19
^{118}Sn	4 14	6—10 6—16	6—10	1.83 1.99	1.09
^{121}Te	6 14	8—11 8—16	8—11	2.95 3.82	1.3
^{136}Ba	8 14	8.3—10.3 8.3—15	8.3—10.3	8.6 14.3	1.67
^{138}Ba	6 14	7—9 7—15	7—9	10.4 15.5	1.5
^{140}Ce	5 14	8—10 8—15	8—10	5.03 6.68	1.33
^{142}Nd	6 14	8.4—11.3 8.4—15.8	8.8—11.3	15.2 23.1	1.52
^{144}Nd	3 14	7—9 7—16	7—9	4.12 9.97	2.4
^{146}Nd	4 14	7.5—9 7.5—15	6.5—9	3.0 6.6	2.2

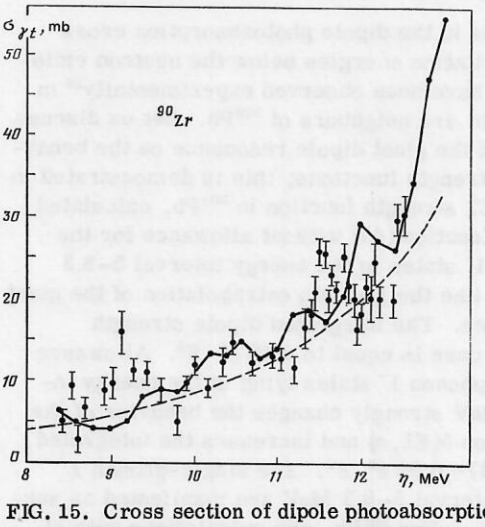

FIG. 15. Cross section of dipole photoabsorption in ^{90}Zr. The points are the experimental data of Ref. 83; the continuous curve is calculated with the wave function (47), and the broken curve is the Lorentz extrapolation of the giant dipole resonance.

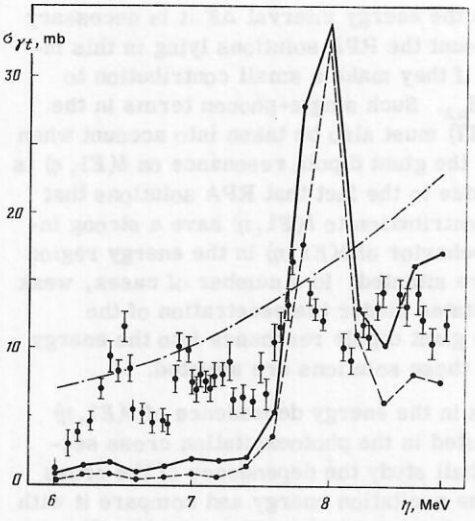

FIG. 16. Dipole photoabsorption cross section in ^{140}Ce. The points are the experimental data of Ref. 87 for natural Ce; the continuous line represents calculations in accordance with the quasiparticle–phonon model with allowance for the giant dipole resonance; the broken line, calculations without allowance for it; and the chain line represents the Lorentz extrapolation of the resonance.

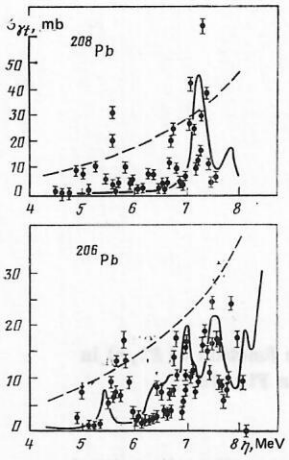

FIG. 17. Photoabsorption cross sections for ^{206,208}Pb. The points are the experimental data of Ref. 88; the continuous curve represents our calculations, and the broken curve is the Lorentz extrapolation of the giant dipole resonance.

energies above 8.2 MeV. The calculated cross sections are smaller than the experimental ones at energies below 7.5 MeV. It is possible that the peaks observed in Ref. 87 at 6.5 and 7 MeV are due to admixtures of other cerium isotopes. In Fig. 16, we also give the results of calculations in which no allowance was made for the phonons forming the giant dipole resonance. It can be seen from the figure that the influence of the resonance on the cross section $\sigma_{\gamma t}$ is not large, though the part played by the resonance increases at excitation energies above 8 MeV. The behavior of the total dipole photoexcitation cross section as a function of the excitation energy differs strongly from the behavior of the Lorentz curve in ^{140}Ce. A similar situation is observed for the photoabsorption cross section for natural barium.[87]

Substructures in the dipole photoabsorption cross sections at excitation energies below the neutron emission threshold have been observed experimentally[88] in many nuclei that are neighbors of ^{208}Pb. Let us discuss the influence of the giant dipole resonance on the behavior of the $E1$ strength functions; this is demonstrated in Fig. 17. The $E1$ strength function in ^{208}Pb, calculated with the wave function (47) without allowance for the single-phonon 1^- states in the energy interval 5–8.3 MeV, behaves like the Lorentz extrapolation of the giant dipole resonance. The integrated dipole strength $\Sigma B(E1)$ in this case is equal to 0.49 $e^2 \cdot F^2$. Allowance for the single-phonon 1^- states lying in the energy interval 5–8.3 MeV strongly changes the behavior of the strength function $b(E1, \eta)$ and increases the integrated strength $\Sigma B(E1) = 0.92\ e^2 \cdot F^2$. The single-phonon 1^- states in the interval 5–8.3 MeV are manifested as substructures in $\sigma_{\gamma t}$. For ^{206}Pb, our calculations with allowance for only the states that form the giant dipole resonance give $\Sigma B(E1) = 0.71\ e^2 \cdot F^2$ for the interval 5–8 MeV. The strength function $b(E1, \eta)$ has structures in this energy interval. The RPA calculations give $\Sigma B(E1) = 0.91\ e^2 \cdot F^2$. Simultaneous allowance for the single-phonon 1^- states in the interval 5–8 MeV and the states of the giant dipole resonance leads to an appreciable redistribution of the dipole strength and the appearance of clearly expressed substructures. In this case, $\Sigma B(E1) = 1.2\ e^2 \cdot F^2$ in the interval 5–8 MeV, which is 30% larger than the value obtained in the RPA calculations. Thus, the influence of the giant dipole resonance on $\sigma_{\gamma t}$ in the region 5–8 MeV in ^{206}Pb is stronger than in ^{208}Pb.

We now discuss the behavior of the cross sections $\sigma_{\gamma t}$ in ^{206,208}Pb in the energy interval 4.5–8 MeV. Our calculations correctly describe the substructure in $\sigma_{\gamma t}$ in ^{208}Pb at energy around 7.3 MeV, but they do not reproduce the substructure around 5.5 MeV, as can be seen from Fig. 18. The $\sigma_{\gamma t}$ calculated for ^{206}Pb exhibit some substructures, which agrees with the experimental data.[88] According to the calculations, there is a

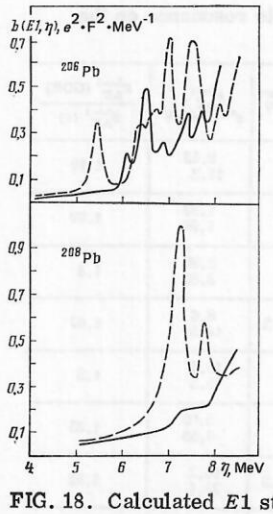

FIG. 18. Calculated $E1$ strength functions in ^{206,208}Pb. The continuous curve represents the calculation without allowance for the single-phonon states in the interval 5–8 MeV; the broken curve is the calculation with allowance for all the single-phonon states, including the giant dipole resonance.

substructure in ^{206}Pb at an energy around 5.5 MeV, which is somewhat lower than the experimental value 5.8 MeV. Our RPA calculations show that in ^{208}Pb there are no single-phonon 1^- states below 6.2 MeV. The first collective single-phonon 1^- state is at 7.3 MeV. The quasiparticle-phonon interaction in ^{208}Pb weakly changes the distribution of the dipole strength at excitation energies below 8 MeV. Therefore, in our calculations there is no substructure in $\sigma_{\gamma t}$ at the energy 5.5 MeV. A single-phonon collective 1^- state is manifested in $\sigma_{\gamma t}$ at 7.3 MeV. Low-lying single-phonon 1^- states can appear if the single-particle spectrum is changed. The distribution of the dipole strength in ^{206}Pb differs radically from ^{208}Pb. The lowest single-phonon 1^- state is at 6.2 MeV, and in the region of 7.3 MeV there are four single-phonon 1^- states. The quasiparticle–phonon interaction appreciably influences the fragmentation of the 1^- states in ^{206}Pb due to the fact that the two-phonon states have there a higher density than they do in ^{208}Pb and they are strongly coupled to the single-phonon states. Because of this, some of the dipole strength is displaced downward and in ^{206}Pb forms the substructure in $\sigma_{\gamma t}$ in the region of 5.5 MeV. The presence of the single-phonon 1^- states and the influence of the giant dipole resonance lead to the appearance of several substructures in the ^{206}Pb cross sections in the energy interval 5–8 MeV, which agrees well with the experimental data.[88]

Investigation of the elastic scattering of photons by ^{208}Pb reveals[89] the existence of substructures in the cross sections at energies $E = 10.04$, 10.6, and 11.27 MeV. Analysis of the photoabsorption cross sections[90] in ^{208}Pb in the energy interval 9.9–11.2 MeV confirms the existence of substructures at $E = 10.04$ and 10.6 MeV. In ^{206}Pb, such substructures were not observed in the interval 9.6–12 MeV. The $E1$ strength functions calculated for the interval 9–12 MeV are shown in Fig. 19, from which it can be seen that in ^{208}Pb there are substructures at $E = 9.7$, 10.5, and 11.3 MeV. According to the calculations, the behavior of $b(E1, \eta)$ at excitation energies below 10.5 MeV in ^{206}Pb is close to the Lorentz extrapolation of the giant dipole resonance. At 11.2 MeV, there is a clearly expressed peak. Thus,

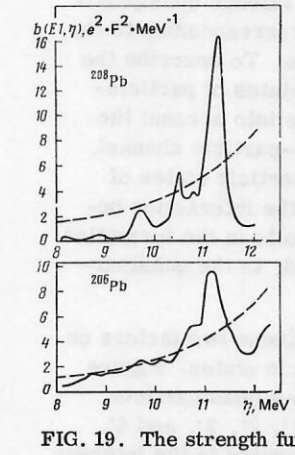

FIG. 19. The strength function $b(E1, \eta)$ for ^{206,208}Pb. The continuous curve represents our calculations, and the broken curve is the Lorentz extrapolation of the giant dipole resonance with parameters from Ref. 58.

the difference between the distributions of the dipole strengths in the semimagic nucleus ^{206}Pb and in the magic ^{208}Pb can be understood as an effect of the quasiparticle–phonon interaction.

Even in nuclei that are far from magic there are irregularities in the absorption cross sections. Figure 20 shows the experimental[91] dipole photoabsorption cross section for ^{64}Zn together with our calculation. In the experimental cross section there are irregularities in the region of 13 MeV and the theory reproduces them well. In the experimental and calculated cross sections there are two maxima, although in the calculations they are more clearly expressed and lie 1 MeV below the experimental values. As we have already noted, at such energies it is necessary to take into account more complicated configurations. Overall, the calculation reproduces well the experimental cross section.

Interesting information about the radiative strength functions is obtained from the investigation of (p, γ) reactions.[92 93] In Ref. 93, radiative capture of protons by the ^{63}Cu nucleus was investigated and information was obtained about the radiative strength function of ^{64}Zn at energies 1–3 MeV above the proton separation energy. This corresponds to γ-transition energies of 7–10 MeV. The excitation functions of direct γ transitions to the ground state in ^{64}Zn measured in Ref. 93 and calculated with the radiative $E1$ and $M1$ strength functions obtained in the quasiparticle–phonon model are given in Fig. 21. In absolute magnitude, the calculated values are close to the observed values. Our calculations reveal a pronounced substructure in the region $E_\gamma \approx 9.5$ MeV. Experimentally, one can identify[93] a certain region near $E_\gamma = 9.5$ MeV in which there is a deviation of the excitation function from a smooth energy dependence. In the total cross section of the ^{63}Cu$(p, \gamma)^{64}$Zn reaction measured on the basis of the yield of γ rays with energies above 3 MeV the deviation near $E_\gamma = 9.5$ MeV is expressed more clearly and has a resonance form with a width of about 0.4 MeV. However, the experimental strength of this state is less than the calculated strength. The contribution of the $M1$ transitions is about 10% of the measured cross section, i.e., approximately the same as according to the statistical estimates, but the energy dependence $\sigma^{M1}(p, \gamma)$ has an irregular nature (Fig. 21).

Our investigations have shown that the quasiparticle–phonon model gives a qualitatively correct description

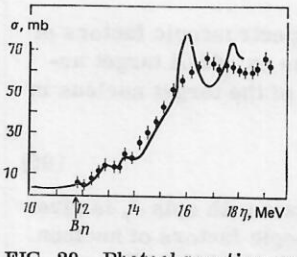

FIG. 20. Photoabsorption cross section in ^{64}Zn. The points are the experimental data of Ref. 91, and the continuous curve represents our calculations.

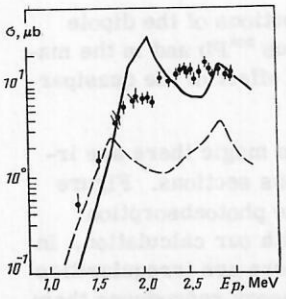

FIG. 21. Excitation function of direct γ transitions in ^{64}Zn to the ground state. The points are the experimental data of Ref. 93; the continuous curve represents the calculation in accordance with the quasiparticle–phonon model for $E1$ transitions; and the broken curve represents the calculation in accordance with the model for $M1$ transitions.

of the distribution of the electromagnetic strength in a wide range of excitation energies and makes it possible to explain and predict the characteristic features of the distribution for individual nuclei. Lorentz extrapolation of the giant dipole resonance to the low-energy region gives a rather crude description of the photoabsorption cross sections, especially in near-magic nuclei. It is shown in Ref. 78 that the Lorentz formula cannot be used for energies below B_n.

5. FRAGMENTATION OF TWO-QUASIPARTICLE STATES

Experimental information about the fragmentation of two-quasiparticle states is obtained from the spectroscopic factors of single-nucleon transfer reactions. However, this is information about only the two-quasiparticle states for which one of the quasiparticles is a valence quasiparticle, i.e., is in a single-particle level corresponding to the ground state of an odd-A target nucleus. It was shown in Refs. 94 and 95 that two-nucleon transfer reactions of the (p,t) type can give more complete information about the fragmentation of the two-quasiparticle states in spherical nuclei. Experimental data from two-nucleon transfer reactions are at present steadily accumulating.[96-98] In the RPA, the magnitude of the two-quasiparticle component $\{j_1 j_2\}$ in a single-phonon state with spin J is determined by $\frac{1}{2}|\psi^{Ji}_{j_1 j_2}|^2$, where $\psi^{Ji}_{j_1 j_2}$ is given by (29). When allowance is made for the quasiparticle–phonon interaction, the single-phonon states are fragmented. The two-quasiparticle component $\{j_1 j_2\}$ with spin J of the state ν described by the wave function (47) is

$$\Phi_{j_1 j_2}(J;\ \eta_\nu) = \frac{1}{2}\Big|\sum_i R_i(J\nu)\,\psi^{Ji}_{j_1 j_2}\Big|^2. \tag{94}$$

We give expressions for the spectroscopic factors of single-nucleon transfer reactions on odd-A target nuclei. We take the wave function of the target nucleus in the form

$$\Psi_{\nu_0}(j_0 m_0) = C_{j_0\nu_0}\alpha^+_{j_0 m_0}\Psi_0. \tag{95}$$

The wave function of the final state with spin J_f is given by Eq. (47). Then the spectroscopic factors of nucleon transfer to subshell j have the following form[29]:

a) for reactions of (d,p) type

$$S_{jj_0}(J_f;\ \eta_\nu) = C^2_{j_0\nu_0}u^2_j\Phi_{jj_0}(J_f;\ \eta_\nu); \tag{96}$$

b) for reactions of (d,t) type

$$S_{jj_0}(J_f;\ \eta_\nu) = C^2_{j_0\nu_0}v^2_j\Phi_{jj_0}(J_f;\ \eta_\nu). \tag{97}$$

If we sum over all spins J_f of the final states that form the single-particle states j_1 and j_2, we obtain

$$S_{jj_0}(\eta_\nu) = \sum_{J_f} S_{jj_0}(J_f;\ \eta_\nu). \tag{98}$$

One frequently uses the expressions

$$S'_{jj_0}(J_f;\ \eta_\nu) = \frac{2J_f+1}{2j_0+1}S_{jj_0}(J_f;\ \eta_\nu); \tag{99}$$

$$S'_{jj_0}(\eta_\nu) = \sum_{J_f}\frac{2J_f+1}{2j_0+1}S_{jj_0}(J_f;\ \eta_\nu). \tag{100}$$

Integrated characteristics of the distribution of the strength of the two-quasiparticle states in the energy interval ΔE are the energy centroids

$$\overline{E}_{jj_0} = \sum_{\nu\in\Delta E}\eta_\nu S'_{jj_0}(\eta_\nu)\Big/\sum_{\nu\in\Delta E}S'_{jj_0}(\eta_\nu) \tag{101}$$

and the total spectroscopic factors

$$N_j = \sum_{\nu\in\Delta E}S'_{jj_0}(\eta_\nu). \tag{102}$$

At intermediate and high excitation energies we calculate instead of (96)–(100) the corresponding strength functions. For this, we use Eq. (80), in which $\Phi_{Ji} = \psi^{Ji}_{jj_0}$. The strength functions for the spectroscopic factors are given by the expressions (96)–(100), in which $\Phi_{jj_0}(J_f;\eta_\nu)$ is replaced by the corresponding strength function $\Phi_{jj_0}(J_f;\eta)$. Besides (101) and (102), the width of the distribution of the states is frequently extracted from the experimental data:

$$\Gamma_{jj_0} = 2{,}35\sigma,\ \sigma^2 = \int_{\Delta E}(\overline{E}_{jj_0}-\eta)^2 S'_{jj_0}(\eta)\,d\eta/N_j. \tag{103}$$

In Ref. 99, the fragmentation of the first two quadrupole and octupole phonons over the low-lying levels in ^{116}Cd, ^{120}Sn, ^{124}Te, ^{134}Xe, and ^{142}Nd is calculated. The fragmentation of the two-quasiparticle components in the region of excitation energies up to 10 MeV is investigated for a number of spherical nuclei in Refs. 29 and 100.

We study the fragmentation of two-quasiparticle states of particle–hole type. We have in mind two-quasiparticle states of the valence-particle–hole and particle–valence-particle type, the valence quasiparticle being in a single-particle level corresponding to the ground state of an odd target nucleus. To describe the fragmentation of two-quasiparticle states of particle–particle type, it is necessary to take into account the residual interactions in the particle–particle channel. The fragmentation of the two-quasiparticle states of particle–hole type is due, first, to the interaction between the quasiparticles, which results in the formation of single-phonon states, and, second, to the quasiparticle–phonon interaction.

We study the influence of each of these two factors on the fragmentation of two-quasiparticle states. Figure 22 shows the fragmentation of the two-quasiparticle state $\{2d_{3/2}, 2d_{5/2}\}$ in ^{92}Zr with $J^\pi = 1^+$, 2^+, 3^+, and 4^+. The corresponding phonons have energies in the interval 4–4.5 MeV, and the component $\{2d_{3/2}, 2d_{5/2}\}$ in them is predominant. It can be seen from the figure that the

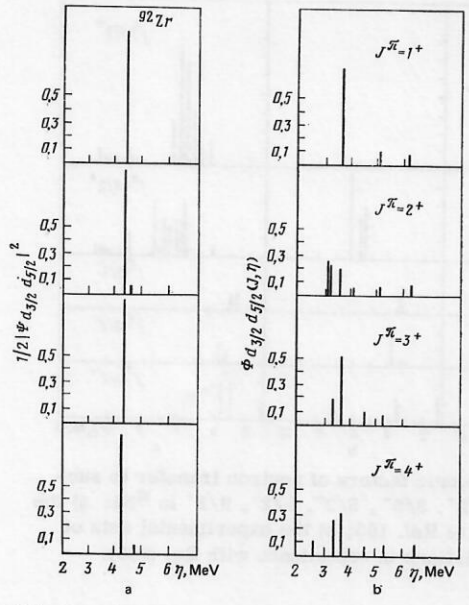

FIG. 22. Fragmentation of the two-quasiparticle state $\{2d_{3/2}, 2d_{5/2}\}$ with $J^{\pi}=1^{+}-4^{+}$ in ^{92}Zr: a) RPA calculations; b) calculations with allowance for the quasiparticle–phonon interaction.

quasiparticle–phonon interaction appreciably enhances the fragmentation of this two-quasiparticle state, and for states with $J^{\pi}=2^{+}$, 3^{+}, and 4^{+} it is large.

The fragmentation of the two-quasiparticle states $\{2d_{3/2}, 1g_{9/2}\}$ with $J^{\pi}=3^{+}$, 4^{+}, 5^{+}, and 6^{+} in ^{120}Sn is shown in Fig. 23. These two-quasiparticle states are appreciably fragmented already in the phonon-formation stage. The fragmentation of the two-quasiparticle states with allowance for the quasiparticle–phonon interaction is shown in the form of the strength function. The total strength of the states in Figs. 23a and 23b is

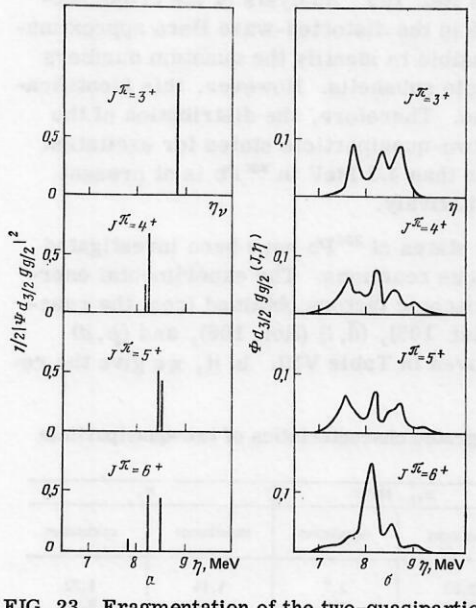

FIG. 23. Fragmentation of the two-quasiparticle state $\{2d_{3/2}, 1g_{9/2}\}$ with $J^{\pi}=3^{+}-6^{+}$ in ^{120}Sn: a) RPA calculations; b) strength functions calculated with allowance for the quasiparticle–phonon interaction.

the same. It can be seen from the figure that the quasiparticle–phonon interaction leads to a further and stronger fragmentation of the two-quasiparticle states. The main fraction of the strength of the $\{2d_{3/2}, 1g_{9/2}\}$ states is concentrated in the region 7–9 MeV. The spec-spectroscopic factors $S'_{jj_0}(J_f; \eta_\nu)$ for the configuration $\{2p_{3/2}, 1g_{9/2}\}$ with $J^{\pi}_f = 3^{-}$ in ^{62}Ni, calculated in the RPA and with the wave function (47), are given in Fig. 24. The main part of the two-quasiparticle strength is distributed over three RPA roots in the energy interval 6–8 MeV. Allowance for the quasiparticle–phonon interaction strengthens the fragmentation of the state $\{2p_{3/2}, 1g_{9/2}\}$.

The considered examples show that the quasiparticle–phonon interaction strongly influences the distribution of the strength of the two-quasiparticle states of spherical nuclei at excitation energies greater than 3–4 MeV.

We consider the fragmentation of two-quasiparticle states of particle–valence-particle type in ^{92}Zr and ^{62}Ni. We compare the results of the calculations of Ref. 29 with the experimental data of Refs. 101 and 102 for the spectroscopic factors of the ^{91}Zr$(d,p)^{92}$Zr reaction. In the experiments, the spins of the final states were not determined, and the spectroscopic factors $S'_{jj_0}(\eta_\nu)$ are given in Refs. 101 and 102 for all possible values of J_f of each two-quasiparticle state. The spectroscopic factors $S'_{jj_0}(\eta_\nu)$ calculated in accordance with Eq. (100) and the corresponding experimental data are shown in Fig. 25. As can be seen from Fig. 25, the spectroscopic factors obtained in these experimental studies differ strongly. The integrated characteristics of the distribution of the strength of the two-quasiparticle states in ^{92}Zr are given in Table VI. We discuss the specific features of the fragmentation of the two-quasiparticle states in ^{92}Zr. The state $\{2d_{5/2}, 2d_{5/2}\}$, in which both quasiparticles are at the Fermi level, is fragmented in the energy interval 1–3 MeV. Experimentally, a large fraction of the sum-rule limit for the strength of this state is observed. In our calculations, this sum rule is exhausted to more than 50%. This is due to the value of the coefficient $u^2_{d_{5/2}} = 0.75$. The theory correctly describes the fragmentation of the two-quasiparticle states $\{3s_{1/2}, 2d_{5/2}\}$ and $\{2d_{3/2}, 2d_{5/2}\}$. The configuration $\{1g_{7/2}, 2d_{5/2}\}$ is more strongly concentrated in the region 3–4 MeV than it is experimentally. With increasing excitation energy, the observation of individual states becomes difficult. Therefore, only a small fraction of the strength of the state $\{1h_{11/2}, 2d_{5/2}\}$ is ob-

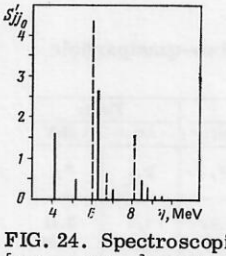

FIG. 24. Spectroscopic factors $S'_{jj_0}(J_f; \eta_\nu)$ for the $\{1g_{9/2}, 2p_{3/2}\}$ configuration with $J^{\pi}_f = 3^{-}$ in ^{62}Ni. The broken lines represent RPA calculations; the continuous lines, calculations with the wave function (47).

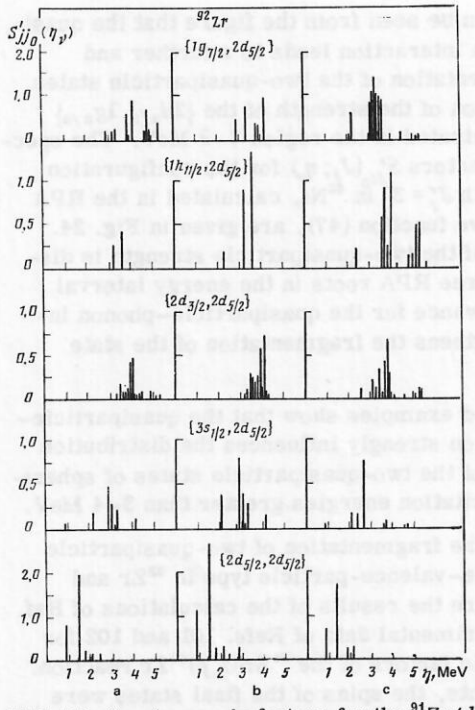

FIG. 25. Spectroscopic factors for the $^{91}Zr(d,p)^{92}Zr$ reaction: a) the experimental data of Ref. 101; b) the experimental data of Ref. 102; c) calculations in accordance with Eq. (100).

served experimentally. Our calculations show that an appreciable fraction of the strength of this state lies at energies greater than 4 MeV. Overall, the experimental data and our calculations give similar pictures of the fragmentation of the two-quasiparticle states in ^{92}Zr. The calculated integrated characteristics agree with the corresponding experimental data.

We discuss the distribution of the strength of the two-quasiparticle states in ^{62}Ni. The experimental data of Refs. 103 and 104 for the spectroscopic factors $S'_{jj_1}(J_f;\eta_\nu)$ of neutron transfer to different subshells j in ^{62}Ni and the calculations of Ref. 100 are shown in Fig. 26. As can be seen from this figure, the spectroscopic factors obtained in Refs. 103 and 104 differ appreciably. Overall, our calculations and the experimental data give similar pictures of the fragmentation of the two-quasiparticle states in ^{62}Ni. The quasiparticle–phonon model correctly describes the enhancement of the fragmentation with increasing excitation energy. The integrated characteristics of the distribution of the strength

TABLE VI. Integrated characteristics of two-quasiparticle states in ^{92}Zr.

$\{jj_0\}$	Experiment				Theory	
	ΔE=0–5.4 MeV [102]		ΔE=0–4.9 MeV [101]		ΔE=0–5.4 MeV	
	$\bar{E}_{jj_0}$	N_j	$\bar{E}_{jj_0}$	N_j	$\bar{E}_{jj_0}$	N_j
$\{2d_{5/2}, 2d_{5/2}\}$	1.43	3.79	1.35	4.62	1.5	3.11
$\{3s_{1/2}, 2d_{5/2}\}$	2.94	1.30	2.93	2.28	2.9	1.70
$\{2d_{3/2}, 2d_{5/2}\}$	4.087	2.59	3.763	3.65	3.8	3.0
$\{1g_{7/2}, 2d_{5/2}\}$	4.207	4.55	3.674	2.99	3.3	6.6
$\{1h_{11/2}, 2d_{5/2}\}$	>3.44	0.66	>3.31	2.84	4.8	5.2
$\{2f_{7/2}, 2d_{5/2}\}$	>4.53	0.39	>3.18	0.23	5.11	1.7

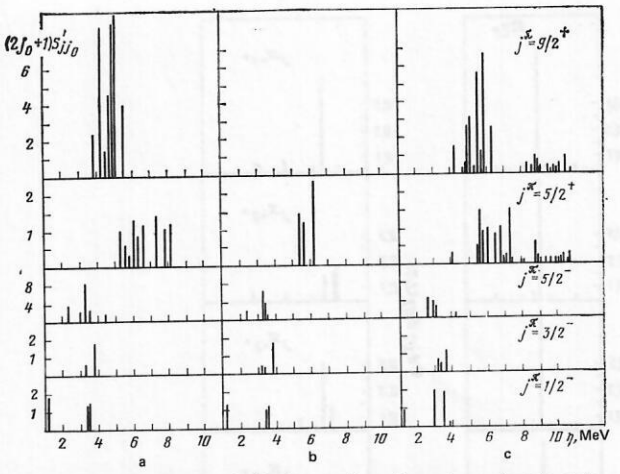

FIG. 26. Spectroscopic factors of neutron transfer to subshells with $J^\pi=1/2^-$, $3/2^-$, $5/2^-$, $5/2^+$, $9/2^+$ in ^{62}Ni: a) the experimental data of Ref. 103; b) the experimental data of Ref. 104; c) calculations in accordance with Eq. (100).

of the two-quasiparticle states for ^{62}Ni are given in Table VII for the energy interval ΔE = 0–8.2 MeV investigated experimentally in Ref. 103. In the brackets in Table VII we also give the results of calculations for $j1g_{9/2}$ and $2d_{5/2}$ for the interval of energies up to the neutron binding energy B_n = 10.6 MeV. The experimental data and our calculations show that 50–60% of the strength of the $\{2p_{3/2}, 2d_{5/2}\}$ configuration is displaced into the continuum.

Thus, the quasiparticle–phonon model gives a correct description of the fragmentation of states of the particle–valence-particle type.

For the example of the ^{206}Pb nucleus we consider the fragmentation of states of the valence-particle–hole type excited in single-nucleon transfer reactions. Experimental data for the spectroscopic factors of $^{207}Pb(^3He,\alpha)^{206}Pb$ reactions in a wide range of energies were obtained in Ref. 105. Analysis of the cross sections of Ref. 105 in the distorted-wave Born approximation made it possible to identify the quantum numbers of the neutron hole subshells. However, this identification is not unique. Therefore, the distribution of the strength of the two-quasiparticle states for excitation energies greater than 4.3 MeV in ^{206}Pb is at present known only qualitatively.

The low-lying states of ^{206}Pb have been investigated in detail in various reactions. The experimental energies and spectroscopic factors obtained from the reactions $(^3He,\alpha)$ (Ref. 105), $(\vec{d},t)$ (Ref. 106), and (p,d) (Ref. 107) are given in Table VIII. In it, we give the re-

TABLE VII. Integrated characteristics of two-quasiparticle states in ^{62}Ni.

$\{jj_0\}$	E_{jj_0}, MeV		N_j	
	experiment	calculation	experiment	calculation
$\{2p_{1/2}, 2p_{3/2}\}$	2.52	2.7	1.14	1.32
$\{1f_{5/2}, 2p_{3/2}\}$	3.14	2.8	4.44	3.3
$\{1g_{9/2}, 2p_{3/2}\}$	4.73	5.2 (6.3)	9.7	6.1 (8.2)
$\{2d_{5/2}, 2p_{3/2}\}$	6.72	6.2 (7.2)	2.26	2.3 (3.2)

TABLE VIII. Energies and spectroscopic factors $S'_{jj_0}(J_f, \eta_v)$ for low-lying states in ^{206}Pb (references are indicated by square brackets).

$\{jj_0\}$	J_f^π	η_v, MeV	$S'_{jj_0}(J_f, \eta_v)$				
		experiment	calculation	[105] (^{3}He, α)	[106] (d, t)	[107] (p, d)	calculation
$\{2f_{7/2}, 3p_{1/2}\}$	4^+	1,684	1,9	0,22	—	0,17	0,16
	4^+	1,998	2,2	0,2	—	0,14	0,23
	4^+	2,928	2,9	3,02	3,45	3,97	2,9
	3^+	3,122	3,0	2,60	2,69	3,37	2,6
	4^+	3,519	3,9	0,23	—	0,21	0,16
$\{1i_{13/2}, 3p_{1/2}\}$	7^-	2,200	1,8	4,25	5,5	7,05	6,4
	6^-	2,384	2,1	3,60	5,0	6,47	5,4
	7^-	2,865	3,0	0,2	—	0,32	0,24
$\{1h_{9/2}, 3p_{1/2}\}$	4^+	4,008	3,9	1,85	—	4,3	3,7
	5^+	4,116	4,0	2,55	—	5,00	4,8

sults of our calculations with the wave function (47), which are close to calculations in the RPA. It can be seen from the table that there is an appreciable spread between the different experimental data. Our calculated energies of the low-lying states agree well with the experimental data. For states with large values of $S'_{jj_0}(J_f; \eta_v)$ we obtain results close to the other theoretical calculations of Refs. 108 and 109. Our results and the experimental data for $N_j/(2j+1)$, which characterizes the extent to which the sum-rule limit (equal to 1) for the strength of the configurations is exhausted, are shown in Table IX. Analysis of the data on the ^{207}Pb$(p,d)^{206}$Pb reaction shows that for the states $\{2f_{7/2}, 3p_{1/2}\}$, $\{1i_{13/2}, 3p_{1/2}\}$, $\{1h_{9/2}, 3p_{1/2}\}$ with energy less than 4.2 MeV the sum-rule limit is exhausted to within a few percent. It was found to be exhausted less in the (^{3}He, α) reaction. The results of our calculations are closest to the data obtained from the (d,t) reaction.

The distribution of the strength of the higher-lying two-quasiparticle states is known only from the (^{3}He, α) reaction. These experimental data and the results of the calculations are shown in Table X. The extent to which the sum-rule limit is exhausted in the process is indicated in the brackets. The calculations agree qualitatively with the experimental data of Ref. 105.

We discuss the fragmentation of the $\{3p_{1/2}, 1h_{11/2}\}$ configuration in ^{206}Pb. In the cross section of the ^{207}Pb(^{3}He, α)^{206}Pb reaction in the energy interval 7.4–10.6 MeV a peak with fine structure is observed. The presence of this peak is due to the fragmentation of the $\{3p_{1/2}, 1h_{11/2}\}$ configuration, which includes a deep hole state $1h_{11/2}$. The spectroscopic factors shown in Table X were obtained for the states of the fine structure. The total strength of these states is about 35% of the total strength of the $\{3p_{1/2}, 1h_{11/2}\}$ configuration. Our calculated strength is twice the experimental. In practice, the measured experimental strength is a lower

TABLE IX. The extent to which the sum-rule limit is exhausted for low-lying states in ^{206}Pb.

$\{jj_0\}$	$N_j/(2j+1)$			
	experiment			calculation
	(^{3}He, α)	(d, t)	(p, d)	
$\{2f_{7/2}, 3p_{1/2}\}$	0.78	0.77	0.99	0.76
$\{1i_{13/2}, 3p_{1/2}\}$	0.58	0.75	0.98	0.86
$\{1h_{9/2}, 3p_{1/2}\}$	0.44	—	0.93	0.85

TABLE X. Distribution of the strength of the two-quasiparticle states in ^{206}Pb.

$\{jj_0\}$	ΔE, MeV	N_j	
		experiment	calculation
$\{2f_{7/2}, 3p_{1/2}\}$	0—4.33	6.27	6.2
	4.33—7.4	0.55	1.3
		6.82 (85 %)	7.5 (94 %)
$\{1i_{13/2}, 3p_{1/2}\}$	0—4.33	8.05	12.5
	4.33—7.4	2.8	0.7
		10.85 (78%)	13.2 (94 %)
$\{1h_{9/2}, 3p_{1/2}\}$	0—4.33	4.4	8.5
	4.33—7.4	1.8	1.2
		6.2 (62 %)	9.7 (97 %)
$\{1h_{11/2}, 3p_{1/2}\}$	7.4—7.9	0.69	0.83
	7.9—8.68	1.1	4.56
	8.68—9.29	0.9	2.02
	9.29—10.59	1.35	0.96
		4.04 (34 %)	8.37 (70 %)

bound. A similar situation obtains for the fragmentation of the $1h_{11/2}$ subshell in ^{207}Pb. The fine-structure states exhaust about 45% of the sum-rule limit.[105] However, analysis[95] of the spectroscopic strength localized in the complete peak gives 71%, which agrees well with calculations in the quasiparticle–phonon model[44] and other calculations.[39] For the energy centroid of the $\{3p_{1/2}, 1h_{11/2}\}$ states in ^{206}Pb the calculations give $\overline{E}_{jj_0} = 8.6$ MeV, the experimental value being $\overline{E}_{jj_0} = 8.9$ MeV. Because of the complicated structure of the peak, it is difficult to determine the width of the distribution by approximating it by a Gaussian curve. Experimentally,[105] the estimate $\Gamma_{jj_0} \sim 4$ MeV is obtained in ^{206}Pb. Our calculations give $\Gamma_{jj_0} = 2$ MeV. At the present time, the fragmentation of the two-quasiparticle states is being investigated in the ^{208}Pb$(\alpha, ^6$He$)^{206}$Pb reaction at Orsay.[110]

In recent years, experimental data on the fragmentation of the two-quasiparticle states in the Cd and Sn isotopes have been obtained from study of the (p,d) and (p,t) reactions.[95,111] In the cross sections of the (p,t) reaction on the even–even Cd and Sn isotopes resonancelike structures are observed at excitation energies 7–9 MeV. The peaks in the cross sections are due to the excitation of states including a valence particle and a deep hole.[112] It is also assumed that there is a certain admixture of two-hole states. The investigation[111,112] of the (p,d) reaction on ^{111,113}Cd and ^{117,119}Sn reveals the existence of clearly expressed resonancelike structures in the cross sections at excitation energies 6.7–9.0 MeV. The dependences of the energies and widths of the peaks on the mass number A in the cross sections of single-nucleon and two-nucleon transfers are very similar. At the same time, the widths of such structures in (p,d) reactions are appreciably less than those observed in the (p,t) reactions. The fragmentation of the two-quasiparticle states in the Sn isotopes was investigated in the framework of the quasiparticle–phonon model in Ref. 29. The strength functions of the states $\{1g_{7/2}, 1g_{9/2}^{-1}\}$, $\{3s_{1/2}, 1g_{9/2}^{-1}\}$, $\{2d_{3/2}, 1g_{9/2}^{-1}\}$, $\{1h_{11/2}, 1g_{9/2}^{-1}\}$ for the Sn isotopes are shown in Fig. 27. The arrows indicate the energies of the peaks observed in the cross sections of the (p,t) reaction. In single-nucleon transfer reactions of the (p,d) type on odd-A targets, two-quasipar-

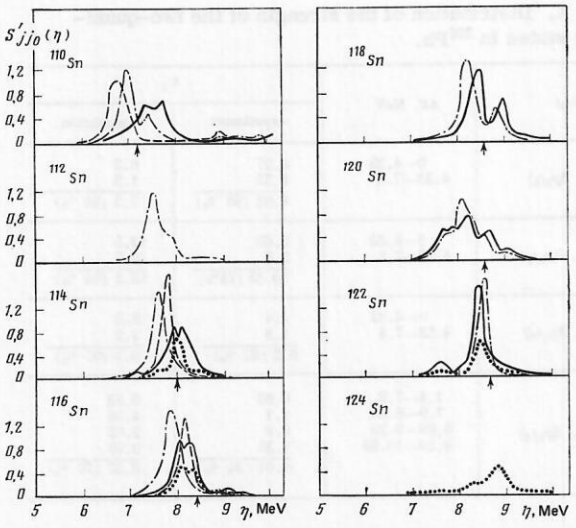

FIG. 27. Strength functions $S'_{jj_0}(\eta)$ for even–even Sn isotopes. The continuous curve is for the $\{2d_{3/2}, 1g_{9/2}\}$ configurations, the broken curve for the $\{1g_{7/2}, 1g_{9/2}\}$, the chain curve for the $\{3s_{1/2}, 1g_{9/2}\}$, and the dotted curve for the $\{1h_{11/2}, 1g_{9/2}\}$ configuration.

ticle states of the valence-particle–hole type must be excited. Such configurations are $\{1g_{7/2}; 1g^{-1}_{9/2}\}$ in ^{110}Sn, $\{3s_{1/2}, 1g^{-1}_{9/2}\}$ in ^{112,114,116,118}Sn, $\{2d_{3/2}, 1g^{-1}_{9/2}\}$ in ^{120}Sn, and $\{1h_{11/2}, 1g^{-1}_{9/2}\}$ in ^{122,124}Sn. In the (p,t) reaction, there are also excited two-hole states (for example, $\{1g^{-1}_{9/2}, 1g^{-1}_{9/2}\}$) and states including a particle in a level near the Fermi surface and a deep hole (for example, $\{2d^{-1}_{5/2}, 1g^{-1}_{9/2}\}$ in ^{114}Sn).

The energy centroids $\overline{E}_{jj_0}$ and the widths Γ_{jj_0} for states excited in the (p,d) and (p,t) reactions leading to the formation of the same final even–even nuclei are shown in Fig. 28 for the different Sn isotopes. Calculations of $\overline{E}_{jj_0}$ and Γ_{jj_0} are given for the (p,d) reaction for configurations including a valence particle and a $1g_{9/2}$ hole for the energy interval $\Delta E = 2$ MeV. As can be seen from Fig. 28, the calculated energy centroids $\overline{E}_{jj_0}$ agree well with the experimental data from the (p,d) reaction. The calculated energies $\overline{E}_{jj_0}$ lie somewhat lower than the energies of the peaks excited in the (p,t) reaction. The energy $\overline{E}_{jj_0}$ increases with increasing A because of the lowering of the $1g^{-1}_{9/2}$ hole state relative to the Fermi surface. The calculated values of $\overline{E}_{jj_0}$ for the two-quasiparticle $\{3s_{1/2}, 1g^{-1}_{9/2}\}$ states in ^{116}Sn and ^{118}Sn are 7.8 and 8.1 MeV, respectively. According to the calculations of Ref. 26, the energies of the $1g^{-1}_{9/2}$ states in ^{115}Sn and ^{117}Sn are 5.5 and 5.6 MeV. The difference between the energy centroids in the odd and even–even isotopes is 2.3 and 2.5 MeV, respectively, which is very close to the experimental values.[95,112] Thus, our calculations make it possible to explain the difference between the energy centroids of the hole states of odd-A and even–even isotopes of Sn.

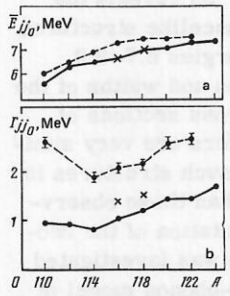

FIG. 28. Energy centroids $\overline{E}_{jj_0}$ (a) and widths Γ_{jj_0} (b) for even–even Sn isotopes. The mass number A refers to the final nucleus; the points joined by the broken line are the experimental data of Ref. 112 for the (p,t) reaction; the crosses are the experimental data of Ref. 112 for the (p,d) reaction; the points joined by the continuous line represent our calculations for the (p,d) reaction.

The Γ_{jj_0} calculated for the (p,d) reaction are somewhat lower than the experimental values. They have a characteristic dependence on A. Such a dependence of Γ_{jj_0} on A is explained, first, by the change in the position of the $1g_{9/2}$ subshell with respect to the Fermi surface and, second, by the change with A of the spin j_0 corresponding to the ground state of the odd-A target nucleus. If j_0 has a large value, then a two-quasiparticle $\{j, j_0\}$ configuration with many values of the spin is excited, which leads to an increase in the width Γ_{jj_0}. Indeed, in ^{110}Sn in the (p,d) reaction the $\{1g_{7/2}, 1g^{-1}_{9/2}\}$ configuration is excited with spin values from 1^+ to 8^+. The width Γ_{jj_0} decreases somewhat in $^{112-116}$Sn, since the $\{3s_{1/2}, 1g^{-1}_{9/2}\}$ configuration is excited with the two spin values 4^+ and 5^+. In ^{120}Sn, the excited $\{2d_{3/2}, 1g^{-1}_{9/2}\}$ configuration has spin values $J^\pi = 3^+-6^+$, and Γ_{jj_0} is somewhat increased. In ^{124}Sn, the $\{1h_{11/2}, 1g^{-1}_{9/2}\}$ configuration is excited and strongly fragmented over the interval 7–10 MeV. The increase in the width Γ_{jj_0} with increasing A due to the enhancement of the fragmentation of the $\{3s_{1/2}, 1g^{-1}_{9/2}\}$ states is demonstrated in Fig. 27. The results of our calculations for $\overline{E}_{jj_0}$ and Γ_{jj_0} and the available experimental data for the (p,d) reaction are given in Table XI. Our calculated Γ_{jj_0} are somewhat lower than the experimental values, but the ratios of the widths for ^{118}Sn and ^{116}Sn are described well. In the even–even Sn isotopes, 70–80% of the strengths of the two-quasiparticle valence-particle–hole states $1g_{9/2}$ is localized in an interval 1–2 MeV at excitation energies 7–9 MeV. As can be seen from Fig. 28, the dependence of $\overline{E}_{jj_0}$ and Γ_{jj_0} on the mass number A calculated for the (p,d) reaction on the odd-A isotopes of Sn is very similar to the one obtained from the experimental data for the (p,t) reaction. This is explained by the fact that in the (p,t) reaction configurations of the valence-particle–hole type $1g_{9/2}$ are also

TABLE XI. Energy centroids $\overline{E}_{jj_0}$ and widths Γ_{jj_0} for configurations excited in (p,d) reactions.

Nucleus	$\overline{E}_{jj_0}$			Γ_{jj_0}		
	experiment	reference	calculation	experiment	reference	calculation
^{110}Sn	—	—	6.7	—	—	0.94
^{112}Cd	6.95	[113]	7.5	—	—	1.2
^{112}Sn	—	—	7.5	—	—	0.9
^{114}Sn	—	—	7.6	—	—	0.8
^{116}Sn	7.79	[112]	7.8	1.38	[112]	1.0
	8.0	[113]	—	—	—	—
^{118}Sn	8.14	[112]	8.1	1.6	[112]	1.2
	8.25	[113]	—	—	—	—
^{120}Sn	—	—	8.2	—	—	1.4
^{122}Sn	—	—	8.4	—	—	1.5
^{122}Te	—	—	7.6	—	—	1.1
^{124}Sn	—	—	8.5	—	—	1.7

excited. This was pointed out in Ref. 114. In ^{110}Sn, the $\{3s_{1/2}, 1g_{9/2}^{-1}\}$, $\{2d_{3/2}, 1g_{9/2}^{-1}\}$, and $\{2d_{5/2}, 1g_{9/2}^{-1}\}$ configurations lie at energies 6–8 MeV, i.e., at the same energies at which the peak in the (p,t) reaction is observed. The excitation in the (p,t) reaction of these configurations together with the $\{1g_{7/2}, 1g_{9/2}^{-1}\}$ configuration increases the width Γ_{jj_0} compared with the case of the (p,d) reaction. The increase in the widths Γ_{jj_0} in the (p,t) reactions on the heavy Sn isotopes is due to the increased fragmentation of the $\{2d_{3/2}, 1g_{9/2}^{-1}\}$ and $\{1h_{11/2}, 1g_{9/2}^{-1}\}$ states.

Thus, it can be concluded that the resonancelike structures observed in the (p,t) reaction on the isotopes $^{110-124}$Sn at energies 7–9 MeV are due to excitation of the $\{1g_{7/2}, 1g_{9/2}^{-1}\}$, $\{3s_{1/2}, 1g_{9/2}^{-1}\}$, $\{2d_{3/2}, 1g_{9/2}^{-1}\}$, $\{2d_{5/2}, 1g_{9/2}^{-1}\}$ configurations. In accordance with our calculations, these states are fragmented in an energy interval 6.5–9.0 MeV. The resonancelike structures excited in the two-nucleon transfer reactions may have a substructure. Indeed, in the ^{116}Sn$(\alpha, ^6$He$)^{114}$Sn reaction there are observed[97] a broad structure (Γ_{jj_0}=2.2 MeV) in the region of excitation energy $E \approx 8$ MeV and two substructures at 7.45 and 8.3 MeV. Analysis of the angular distribution shows that in this reaction $J_f^\pi = 6^+$ states are largely excited, good description of the angular distribution of the group of states with energy 7.45 MeV requiring us to assume that these states also include states with $J_f^\pi = 8^+$. Calculations in the quasiparticle–phonon model[29] give the energy centroids $\overline{E}_{jj_0}$ = 7.6 MeV for the $\{1g_{7/2}^{-1}, 1g_{9/2}^{-1}\}$ configuration, $\overline{E}_{jj_0}$ = 8.2 MeV for the $\{2d_{5/2}^{-1}, 1g_{9/2}^{-1}\}$ configuration, and $\overline{E}_{jj_0}$ = 8.0 MeV for the $\{2d_{3/2}, 1g_{9/2}^{-1}\}$ configuration. In the $(\alpha, ^6$He) reaction one observes the strongest excitation[97] of states accompanied by the transfer of two neutrons with $l_1 = 6$. A lower group of states corresponds to the $\{1g_{7/2}^{-1}, 1g_{9/2}^{-1}\}$ configuration, which may have the values $J_f^\pi = 6^+$ and 8^+. An upper group of states corresponds to the $\{1g_{9/2}^{-1}, 2d_{5/2\ 3/2}\}$ configuration with $J_f^\pi = 6^+$. Thus, the observation of two groups of states, the lower group being a mixture of states with $J_f^\pi = 6^+$ and 8^+, in ^{114}Sn has a natural explanation in the framework of the quasiparticle–phonon model. The experimental energy centroids 7.45 and 8.3 MeV agree well with the values predicted in Ref. 29 (7.6 and 8.2 MeV).

Besides the Sn isotopes, $\overline{E}_{jj_0}$ and Γ_{jj_0} are calculated in Ref. 29 for some Cd and Te isotopes. They also agree well with the available experimental data.

One further characteristic determined by the fragmentation of the two-quasiparticle states is the neutron strength functions of even–even spherical nuclei. The neutron strength functions are important characteristics of nuclei at excitation energies above the neutron binding energy B_n. The most complete experimental data on the neutron functions are collected together in Ref. 115.

In the case when a neutron with orbital angular momentum l is absorbed by a target nucleus with spin I_0, the neutron strength function is determined by

$$S_l = \sum_{Jj} g(J)\, S_l^{Jj}, \tag{104}$$

where $g(J) = 2J + 1/2(2I_0 + 1)(2l + 1)$ is the statistical weight, and S_l^{Jj} is the value of the l-strength function with given value $J = I_0 + l + 1/2 = I_0 + j$ of the spin of the compound nucleus in channel j:

$$S_l^{Jj} = \frac{\Gamma_{s.p}^{0l}}{\Delta E} \int_{\Delta E} d\eta \gamma_{Jj}^2(\eta), \tag{105}$$

$$\gamma_{Jj}^2(\eta) = b(\Phi, \eta) \quad \text{for} \quad \Phi_{Ji} = \sum_n u_{nlj} \psi_{nlj,\, n_0 i_0 I_0}^{Ji}. \tag{106}$$

Here, u_{nlj} is the coefficient of a Bogolyubov transformation, $b(\Phi, \eta)$ is determined in accordance with Eq. (80), and ψ^{Ji} are phonon amplitudes [Eq. (29)]. In Eq. (106), we have summed over the principal quantum number of the single-particle state. To estimate the reduced single-particle widths $\Gamma_{s.p}^{0l}$ in the case of the Woods–Saxon potential, we use the semiempirical formula proposed in Ref. 116:

$$\Gamma_{s.p}^0 = 2kR \frac{\hbar^2}{MR^2\sqrt{E}}(1 + 6.7d^2), \tag{107}$$

where k is the neutron wave number, R is the radius of the nucleus, and d is the diffuseness parameter of the Woods–Saxon potential. For the nuclei we consider, $\Gamma_{s.p}^0 \sim 50/A^{1/3}$ keV. The experimental data of Refs. 115 and 117 and the results of our calculations[81] for the s-wave strength functions are given in Table XII. The calculations describe rather well the experimental data and, overall, correctly reproduce the behavior of S_0 as a function of A. The results of our calculations for nuclei with $A \approx 90$ are very close to the results of Ref. 118. The results of the calculations for the p-strength functions S_1, which also agree well with the experiments[115 117] are given in Table XIII. In the ^{54}Cr nucleus, the large value of S_0 and the small value of S_1 are simultaneously described.

The spin dependence of the neutron strength functions has frequently been discussed in the literature. The most complete experimental data can be found in Ref. 122. In the case when an s neutron is absorbed by a nucleus with an odd number of nucleons with spin I_0, compound states with $J = I_0 \pm \frac{1}{2}$ are excited. For each value of the spin J, the strength function can have values S^+ and S^- ($S^\pm = S_0^{I_0 \pm 1/2, 1/2}$) not equal to each other. The statistical analysis of the experimental data made in Ref. 119 shows that for the overwhelming number of nuclei $S^+ = S^-$ and the deviations from this are purely random. However, in some nuclei S^+ differs appreciably from S^-. Experiments aimed at direct determination of the difference $S^+ - S^-$ were made in Ref. 120 for a number of nuclei in the region of the rare earths. To within the experimental errors, $S^+ = S^-$.

In the framework of the quasiparticle–phonon model there is a fundamentally new possibility of theoretical

TABLE XII. The s-wave strength functions of even–even spherical nuclei.

Target nucleus	I_0^π	B_n, MeV	$S_0 \cdot 10^4$	
			experiment	calculation
^{53}Cr	3/2$^-$	9.72	5.03±0.06	4.5
^{61}Ni	3/2$^-$	10.6	3.0±0.8	2.5
^{73}Ge	9/2$^+$	10.2	1.5±0.4	1.6
^{87}Sr	9/2$^+$	11.1	0.26±0.06	0.88
^{91}Zr	5/2$^+$	8.63	0.9±0.3	9.6
^{95}Mo	5/2$^+$	9.15	0.48±0.1	0.5
^{97}Mo	5/2$^+$	8.64	0.37±0.15	0.8

TABLE XIII. The p-wave strength functions of even–even spherical nuclei.

Target nucleus	I_0^π	B_n, MeV	$S_1 \cdot 10^4$	
			experiment	calculation
^{53}Cr	3/2$^-$	9.72	0.081±0.051	0.08
^{61}Ni	3/2$^-$	10.6	—	0.10
^{143}Nd	7/2$^-$	7.82	1.2±0.5	1.6

TABLE XIV. Spin dependence of s-wave strength functions.

Compound nucleus	$S^+ \cdot 10^4$	$S^- \cdot 10^4$	$2(S^+ - S^-)/(S^+ + S^-)$
^{54}Cr	4.64	4.37	0.06
^{62}Ni	2.46	2.4	0.025
^{88}Sr	0.7	1.1	—0.44
^{92}Zr	0.65	0.58	0.11
^{96}Mo	0.55	0.42	0.27
^{98}Mo	0.86	0.75	0.24

investigation of the spin dependence of the neutron strength functions. Using Eqs. (105) and (106), we can readily calculate S^+ and S^-. As can be seen from Fig. 29, $\gamma^2_{J1/2}(\eta)$ have different shapes in their dependence on the excitation energy for different values of J. Therefore, the question of whether S^+ and S^- will be equal depends on the ratios $\gamma^2_{J1/2}(\eta)$ for the two values of J in the region of the neutron binding energy B_n. The values of $\gamma^2_{I_0\pm1/2,1/2}$ are determined by different matrix elements, and they may therefore differ. In Table XIV, we give the results of calculations for S^+ and S^- and the ratio $2(S^+ - S^-)/(S^+ + S^-)$, which characterizes the deviation of S^+ from S^-. A strong difference between the values of S^+ and S^- is not observed, though there is some spin dependence for the nuclei Zr and Mo. We obtain the strongest spin dependence for ^{88}Sr. On the basis of the existing experimental data and the results of the calculations it can be asserted that $S^+ = S^-$ for the majority of nuclei.

In Ref. 121, substructures were found in the energy dependence of the total reduced neutron widths $\Sigma\Gamma^{0l}_{n\nu}$ of ^{208}Pb, measured in the energy interval 0–500 keV above B_n. The available experimental data for $\Sigma\Gamma^{0l}_{n\nu}$ with $l = 0$ and 2 and the results of our calculations[60] are given in Fig. 30. For states with $J^\pi = 1^-$ excited by s-wave neutrons there is a sharp increase in the $\Sigma\Gamma^{00}_{n\nu}$ values at neutron energies of 500 keV. In the calculated energy dependence of $\Sigma\Gamma^{00}_{n\nu}$ there is also a bend, but it is less sharp. In the case of scattering of d-wave neutrons there is also an indication of a presence of substructures.[124] The calculations reveal a sharp, as in the experiment, change in $\Sigma\Gamma^{02}_{n\nu}$ at $E_n \approx 250$ keV for the $d_{3/2}$ state, but in absolute magnitude the calculated $\Sigma\Gamma^{02}_{n\nu}$ lie significantly higher than the experimental data. In the channel with $J^\pi = 2^-$ and 3^- there is also a change in S_2^J at $E_n \approx 300$ and 400 keV, respectively.

The presence of these changes in $\Sigma\Gamma^{0l}_{n\nu}$ in ^{209}Pb is due to the existence of substructures in the fragmentation of the corresponding states. In ^{208}Pb, the s-wave strength function is determined by the fragmentation of the two-quasiparticle state $\{3p_{1/2}, 4s_{1/2}\}$, and the d-wave strength function by the fragmentation of the states $\{3p_{1/2}, 3d_{3/2}\}$ and $\{3p_{1/2}, 3d_{5/2}\}$. In the distribution of the strengths of these states at energies above B_n there are local maxima. As an example, Fig. 31 shows for the two-quasiparticle state $\{3p_{1/2}, 3d_{3/2}\}$ the strength function $b(\Phi, \eta)$ calculated with the wave function (47) and the distribution of the strength over the different roots of the solutions of the RPA equations. It is found that 92% of the strength of this state is concentrated on one level with energy 6.9 MeV, the remainder being distributed over three states. Calculations with the wave function (47) lead to a broader energy spread of the strengths and to the appearance of a local maximum at $\eta = 7.45$ MeV, which is 200 keV above B_n. This local maximum appears in the energy dependence of $\Sigma\Gamma^{02}_{n\nu}$. There are similar substructures in the $s_{1/2}$ and $d_{5/2}$ channels. The division of the strength of the above two-quasiparticle configurations in ^{208}Pb occurs mainly because of the strong coupling to the two-phonon states $\{2^+_1 \otimes 3^-_1\}$ and $\{4^+_1 \otimes 3^-_1\}$, which in our calculations have energies 7.31 and 7.48 MeV, respectively. If possible effects of the substructures are ignored, the value $S_2 \approx 2.8\times10^{-4}$ is obtained in Ref. 124 for the total d-wave strength function in the energy interval 180–400 keV. For the energy interval 200–500 keV, our calculations give values $S_2 \approx 2.0\times10^{-4}$, but if the averaging is over the interval 0–800 keV we obtain $S_2 = 1.4\times10^{-2}$. For S_0,

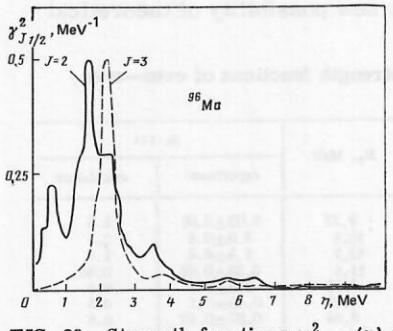

FIG. 29. Strength functions $\gamma^2_{J1/2}(\eta)$ for ^{96}Mo.

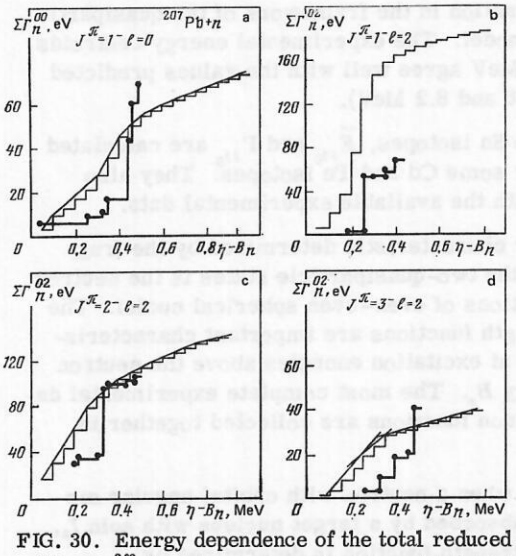

FIG. 30. Energy dependence of the total reduced neutron widths in ^{208}Pb: a) s-wave resonances; b) d-wave resonances; c) d-wave resonances; d) d-wave resonances. The points are the experimental data of Ref. 121, and the continuous lines are the results of our calculations.

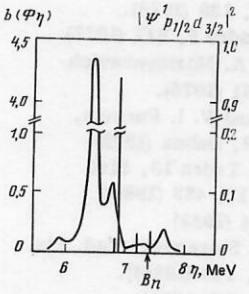

FIG. 31. Calculated distribution of the strength of the two-quasiparticle neutron state $\{3p_{1/2}, 3d_{3/2}\}$ with $J^\pi = 1^-$ in ^{208}Pb. The straight lines are calculations of the distribution of the strength over the different RPA solutions (right-hand scale); the curve represents a calculation of the strength function with allowance for the two-phonon components (left-hand scale). The arrow indicates the position of the neutron binding energy.

the calculations give the value $S_0 = 1.1 \times 10^{-4}$, the experimental value being $S_0 = 1.4 \times 10^{-4}$, if it is estimated without allowance for the substructure.

The foregoing discussion shows that the use of the microscopic approach to calculate the neutron strength functions not only makes it possible to obtain a quantitative description of them without special choice of the parameters, which is valuable in itself, but also gives qualitatively new possibilities (investigation of the spin dependence and the substructures of the neutron strength functions) that are not available at all in standard calculations using the optical model.

CONCLUSIONS

We have given a systematic exposition of the formalism of the quasiparticle–phonon model used to investigate physical characteristics determined by the fragmentation of two-quasiparticle states of even–even spherical nuclei. For specific physical examples such as the problem of describing the properties of giant multipole resonances, neutron and radiative strength functions, and the fragmentation of two-quasiparticle states, we have demonstrated the possibility of successful use of this model. It is clear that the class of such examples can be significantly extended, but this would greatly increase the length of the review.

The circumstance that in the framework of the quasiparticle–phonon model it is possible with a unified set of parameters to obtain a good description simultaneously of many nuclear characteristics in a fairly large region of excitation energies indicates that the model correctly encompasses the main features of nuclear dynamics. In the framework of the model it is possible to calculate a larger class of nuclear characteristics and the cross sections of a larger number of reactions for spherical nuclei with $A > 50$. There are great potential possibilities for the further development of the quasiparticle–phonon model.

[1]V. G. Solov'ev, Vliyanie parnykh korrelyatsiĭ sverkhprovodyashchego tipa na svoĭstva atomnykh yader (Influence of Pairing Correlations of Superconducting Type on the Properties of Nuclei), Gosatomizdat, Moscow (1963); V. G. Soloviev, in: Selected Topics in Nuclear Theory, IAEA, Vienna (1963), p. 233.
[2]V. G. Soloviev, At. Energy Rev. **3**, 117 (1965).
[3]V. G. Soloviev, in: Nuclear Structure, Dubna Symposium, IAEA, Vienna (1968), p. 101.
[4]V. G. Solov'ev, Teoriya slozhnykh yader, Nauka, Moscow (1971); English translation: Theory of Complex Nuclei, Pergamon, Oxford (1976).
[5]V. G. Solov'ev, Izv. Akad. Nauk SSSR, Ser. Fiz. **35**, 666 (1971); **38**, 1580 (1974).
[6]V. G. Soloviev and L. A. Malov, Nucl. Phys. **A196**, 433 (1972).
[7]V. G. Solov'ev, Teor. Mat. Fiz. **17**, 90 (1973).
[8]A. I. Vdovin and V. G. Solov'ev, Teor. Mat. Fiz. **19**, 275 (1974).
[9]G. Kyrchev and V. G. Solov'ev, Teor. Mat. Fiz. **22**, 244 (1975).
[10]A. I. Vdovin, G. Kyrchev, and Ch. Stoyanov, Teor. Mat. Fiz. **21**, 137 (1974).
[11]V. G. Solov'ev, Fiz. Elem. Chastits At. Yadra **9**, 860 (1978) [Sov. J. Part. Nucl. **9**, 343 (1978)].
[12]V. G. Soloviev, Nucleonika **23**, 1149 (1979).
[13]V. G. Solov'ev, Izbrannye voprosy struktury yadra (Selected Topics of Nuclear Structure), Vol. 2, D-9920, JINR, Dubna (1976), p. 146; in: Struktura yadra (Nuclear Structure), D4-80-385, JINR, Dubna (1980), p. 57.
[14]L. A. Malov and V. G. Solov'ev, Fiz. Elem. Chastits At. Yadra **11**, 301 (1980) [Sov. J. Part. Nucl. **11**, 111 (1980)].
[15]V. V. Voronov, in: Neutron Induced Reactions (eds. I. Ribansky and E. Betak), Bratislava (1980), p. 291; A. I. Vdovin, Izv. Akad. Nauk SSSR, Ser. Fiz. **43**, 2018 (1979); Ch. Stoyanov, Izv. Akad. Nauk SSSR, Ser. Fiz. **45**, 1820 (1981).
[16]L. A. Malov, Soobshchenie (Communication) R4-81-816, R4-81-118, JINR, Dubna (1981).
[17]A. I. Vdovin and V. G. Solov'ev, Fiz. Elem. Chastits At. Yadra **14**, 237 (1983) [Sov. J. Part. Nucl. **14**, 99 (1983)].
[18]L. A. Malov and V. G. Soloviev, Nucl. Phys. **A270**, 87 (1976).
[19]A. I. Vdovin *et al.*, Fiz. Elem. Chastits At. Yadra **7**, 952 (1976) [Sov. J. Part. Nucl. **7**, 380 (1976)].
[20]D. Dambasuren *et al.*, J. Phys. G **2**, 25 (1976).
[21]G. Kyrchev *et al.*, Yad. Fiz. **25**, 951 (1977) [Sov. J. Nucl. Phys. **25**, 506 (1977)].
[22]V. G. Soloviev, Ch. Stoyanov, and A. I. Vdovin, Nucl. Phys. **A288**, 376 (1977).
[23]V. V. Voronov, V. G. Solov'ev, and Ch. Stoyanov, Pis'ma Zh. Eksp. Teor. Fiz. **25**, 459 (1977) [JETP Lett. **25**, 430 (1977)].
[24]V. G. Soloviev, Ch. Stoyanov, and V. V. Voronov, Nucl. Phys. **A304**, 503 (1978).
[25]V. G. Soloviev, Ch. Stoyanov, and V. V. Voronov, Phys. Lett. **B79**, 187 (1978).
[26]V. G. Soloviev, Ch. Stoyanov, and A. I. Vdovin, Nucl. Phys. **A342**, 261 (1980).
[27]V. Yu. Ponomarev *et al.*, Nucl. Phys. **A323**, 446 (1979).
[28]A. I. Vdovin *et al.*, Yad. Fiz. **30**, 923 (1979) [Sov. J. Nucl. Phys. **30**, 479 (1979)].
[29]V. G. Soloviev, O. Stoyanova, and V. V. Voronov, Nucl. Phys. **A370**, 13 (1981).
[30]V. G. Solov'ev, O. Stoyanova, and Ch. Stoyanov, Izv. Akad. Nauk SSSR, Ser. Fiz. **44**, 1938 (1980).
[31]O. Stoyanova, Preprint R4-81-477 [in Russian], JINR, Dubna (1981).
[32]V. Yu. Ponomarev, Ch. Stoyanov, and O. Stoyanova, Preprint R4-81-704 [in Russian], JINR, Dubna (1981).
[33]R. V. Jolos *et al.*, Z. Phys. **A295**, 147 (1980); V. G. Soloviev and N. Yu. Shirikova, Z. Phys. **A301**, 263 (1981); Yad. Fiz. **36**, 1376 (1982) [Sov. J. Nucl. Phys. **36**, 799 (1982)].
[34]V. G. Soloviev and Ch. Stoyanov, Nucl. Phys. **A382**, 206 (1982).

[35]V. G. Solov'ev, Teoriya atomnogo yadra. Yadernye modeli (Theory of the Atomic Nucleus. Nuclear Models), Énergoizdat, Moscow (1981).
[36]A. M. Lane, R. G. Thomas, and E. P. Wigner, Phys. Rev. 98, 693 (1955).
[37]A. Bohr and B. R. Mottelson, Nuclear Structure, Vol. 1, Benjamin, New York (1969) [Russian translation published by Mir, Moscow (1979)].
[38]O. Bohigas, A. M. Lane, and J. Martorell, Phys. Rep. 5, 269 (1979).
[39]P. F. Bortignon and R. A. Broglia, Nucl. Phys. A371, 405 (1981).
[40]J. Wambach, V. Mishra, and Li Chu-Hsia, Nucl. Phys. A380, 285 (1982).
[41]R. De Haro, S. Krewald, and J. Speth, Nucl. Phys. A388, 265 (1982).
[42]Kh. L. Molina, I. N. Mikhaĭlov, and R. G. Nazmitdinov, Teor. Mat. Fiz. 42, 253 (1980).
[43]V. A. Chepurnov, Yad. Fiz. 6, 955 (1967) [Sov. J. Nucl. Phys. 6, 696 (1968)]; K. Takeuchi and P. A. Moldauer, Phys. Lett. B28, 384 (1969).
[44]V. V. Voronov and Chan Zui Khung, Izv. Akad. Nauk SSSR, Ser. Fiz. 45, 1909 (1981).
[45]H. P. Morsch *et al.*, Phys. Rev. C 22, 489 (1980); Phys. Rev. Lett. 45, 337 (1980).
[46]G. A. Rinker and J. Speth, Nucl. Phys. A306, 360 (1978).
[47]K. F. Liu and G. E. Brown, Nucl. Phys. A265, 385 (1976).
[48]B. L. Birbrair, Izv. Akad. Nauk SSSR, Ser. Fiz. 43, 2243 (1979).
[49]V. V. Pal'chik, N. I. Pyatov, and S. A. Fayans, Yad. Fiz. 34, 903 (1981) [Sov. J. Nucl. Phys. 34, 504 (1981)].
[50]V. A. Khodel and E. E. Saperstein, Nucl. Phys. A348, 261 (1980).
[51]R. Pitthan *et al.*, Phys. Lett. 33, 849 (1974).
[52]J. Speth and A. Van der Woude, Rep. Prog. Phys. 44, 719 (1981).
[53]F. E. Bertrand, Nucl. Phys. A354, 129 (1981).
[54]B. L. Berman and S. C. Fultz, Rev. Mod. Phys. 47, 713 (1975).
[55]A. I. Vdovin, V. G. Solov'ev, and Ch. Stoyanov, Preprint R4-10033 [in Russian], JINR, Dubna (1976).
[56]A. Lepretre *et al.*, Nucl. Phys. A219, 39 (1974).
[57]A. Lepretre *et al.*, Nucl. Phys. A258, 350 (1976).
[58]A. Veyssiere *et al.*, Nucl. Phys. A159, 561 (1970).
[59]V. G. Soloviev, Ch. Stoyanov, and V. V. Voronov, Preprint E4-81-422 [in English], JINR, Dubna (1981).
[60]V. G. Soloviev, Ch. Stoyanov, and V. V. Voronov, Preprint E4-82-389 [in English], JINR, Dubna (1982).
[61]N. I. Venikov *et al.*, Preprint 3352/2 [in Russian], Institute of Atomic Energy, Moscow (1980).
[62]C. M. Rozsa *et al.*, Phys. Rev. C 21, 1252 (1980).
[63]F. E. Bertrand *et al.*, Phys. Rev. C 22, 1832 (1980).
[64]M. Djalali, Preprint IPNO-T-81-02, Orsay (1981).
[65]H. P. Morsch *et al.*, Phys. Rev. C 22, 489 (1980); Phys. Rev. Lett. 45, 337 (1980).
[66]G. Kühner *et al.*, Phys. Lett. B104, 189 (1981).
[67]W. Knüpfer and M. G. Huber, Phys. Rev. C 14, 2254 (1976).
[68]S. Raman, in: Proc. of the Third Intern. Symposium on Neutron Capture Gamma-Ray Spectroscopy and Related Topics, BNL, New York (1978), p. 193.
[69]J. M. Moss *et al.*, Phys. Rev. Lett. 37, 816 (1976); Phys. Rev. C 18, 741 (1978).
[70]M. N. Haraken *et al.*, Nucl. Phys. A327, 373 (1979).
[71]G. N. Afanasiev *et al.*, Preprint E4-11164 [in English], JINR, Dubna (1978).
[72]R. A. Eramzhyan *et al.*, Nucl. Phys. A290, 397 (1977).
[73]S. Fukuda and Y. Torizuka, Phys. Rev. Lett. B29, 1109 (1972).
[74]R. P. Singhal *et al.*, Preprint, Univ. of Glasgow (1975).
[75]G. A. Bartholomew *et al.*, Adv. Nucl. Phys. 7, 229 (1974).
[76]B. J. Allen *et al.*, Adv. Nucl. Phys. 19, 129 (1978).
[77]M. G. Urin, Fiz. Elem. Chastits At. Yadra 8, 817 (1977) [Sov. J. Part. Nucl. 8, 331 (1977)]; B. A. Martsynkevich and E. A. Rudak, Nucl. Phys. A262, 261 (1976).
[78]S. G. Kadmenskiĭ, V. P. Markushev, and V. I. Furman, Preprint R4-82-210 [in Russian], JINR, Dubna (1982).
[79]Yu. P. Popov, Fiz. Elem. Chastits At. Yadra 13, 1165 (1982) [Fiz. Elem. Chastits At. Yadra 13, 483 (1982)].
[80]M. Carol *et al.*, Phys. Rev. C 23, 1394 (1981).
[81]V. V. Voronov, V. G. Solov'ev, and O. Stoyanova, Yad. Fiz. 31, 327 (1980) [Sov. J. Nucl. Phys. 31, 168 (1980)].
[82]R. J. Balgman *et al.*, Phys. Rev. C 3, 672 (1971).
[83]P. Axel *et al.*, Phys. Rev. C 2, 689 (1970).
[84]R. E. Chrien *et al.*, Phys. Rev. C 9, 1622 (1974).
[85]R. J. Holt and H. E. Jackson, Phys. Rev. C 12, 56 (1975).
[86]R. M. Laszewski *et al.*, Phys. Rev. C 13, 2257 (1976).
[87]Nuclear Physics Research with Electrons from MUSL-2 and MUSL-3 (Dept. of Physics, University of Illinois at Urbana-Champaign, 1977).
[88]R. M. Laszewski and P. Axel, Phys. Rev. C 19, 342 (1979).
[89]R. D. Starr *et al.*, Phys. Rev. C 25, 780 (1982).
[90]Z. W. Bell *et al.*, Phys. Rev. C 25, 791 (1982).
[91]P. Carlos *et al.*, Nucl. Phys. A258, 365 (1976).
[92]B. Erlandsson *et al.*, Nucl. Phys. A343, 197 (1980).
[93]B. A. Nemashkalo *et al.*, Izv. Akad. Nauk SSSR, Ser. Fiz. 44, 1027 (1980); Vopr. At. Nauki Tekh., Ser. Obshch. Yad. Fiz. No. 2 (16), 37 (1981); Yad. Fiz. 36, 280, 1083 (1982) [Sov. J. Nucl. Phys. 36, 163, 633 (1982)].
[94]G. M. Crawley, in: Proc. of the 1980 RCNP Intern. Symposium on Highly Excited States in Nuclear Reactions, Osaka (1980), p. 590.
[95]S. Gales, Nucl. Phys. A354, 193 (1981).
[96]T. Nakagawa *et al.*, Nucl. Phys. A376, 513 (1982).
[97]E. Gerlic *et al.*, Phys. Lett. B117, 20 (1982).
[98]G. M. Crawley *et al.*, Phys. Lett. B109, 8 (1982).
[99]A. I. Vdovin, V. G. Solov'ev, and Ch. Stoyanov, Yad. Fiz. 20, 1131 (1974) [Sov. J. Nucl. Phys. 20, 593 (1975)].
[100]V. V. Voronov and I. P. Zhuravlev, Preprint E4-82-512 [in English], JINR, Dubna (1982).
[101]S. S. Ipson *et al.*, Nucl. Phys. A253, 190 (1975).
[102]T. Borello-Lewin *et al.*, Phys. Rev. C 20, 2101 (1979).
[103]O. Karban *et al.*, Nucl. Phys. A266, 68 (1981).
[104]M. L. Halbert, Nucl. Data Sheets 26, 5 (1976).
[105]J. Guillot *et al.*, Phys. Rev. C 21, 879 (1980).
[106]J. E. Willis *et al.*, Nucl. Phys. A367, 8 (1981).
[107]W. A. Lanford and G. M. Crawley, Phys. Rev. C 9, 646 (1974).
[108]J. B. McGrory and T. T. S. Kuo, Nucl. Phys. A247, 283 (1975).
[109]J. Vary and J. N. Ginocchio, Nucl. Phys. A166, 479 (1971).
[110]S. Gales, Preprint IPNO Ph. 81-05, Orsay (1981).
[111]G. M. Crawley *et al.*, Phys. Rev. C 22, 316 (1980).
[112]G. M. Crawley *et al.*, Phys. Rev. C 23, 589 (1981).
[113]T. Ishimatsu *et al.*, J. Phys. Soc. Jpn. 35, 1579 (1973).
[114]M. Nomura, Prog. Theor. Phys. 59, 1771 (1978).
[115]BNL-325, 3-Ed., Neutron Cross Sections, Vol. 1, Resonance Parameters (1973).
[116]E. Vogt, Rev. Mod. Phys. 34, 723 (1962).
[117]L. A. R. De Musgrove *et al.*, Nucl. Phys. A270, 108 (1976); Preprint AAEC/E401 (1977).
[118]V. K. Sirotkin and Yu. V. Adamchuk, Yad. Fiz. 26, 495 (1977) [Sov. J. Nucl. Phys. 26, 262 (1977)].
[119]L. Lason', Kh. Malétski, and Kh. Faĭkov, Acta Phys. Pol. B8, 1009 (1977).
[120]V. P. Alfimenkov *et al.*, Nucl. Phys. A376, 229 (1982).
[121]D. J. Horen *et al.*, Phys. Rev. C 18, 722 (1978); 20, 478 (1979); 24, 1961 (1981).

Translated by Julian B. Barbour